Jurassic fossil juvenile reveals prolonged life history in early mammals

Elsa Panciroli[1,2]*, Roger Benson[3], Vincent Fernandez[4], Nicholas Fraser[1], Matt Humpage[5], Zhe-Xi-Luo[6], Elis Newham[7,8], and Stig Walsh[1]

1. Natural Sciences Department, National Museums Scotland, Chambers Street, Edinburgh, EH1 1JF, UK
2. University of Oxford Museum of Natural History, Parks Road, Oxford, OX1 3PW, UK
3. American Museum of Natural History, 200 Central Park West, New York, NY 10024, United States
4. European Synchrotron Radiation Facility, 71 Av. des Martyrs, 38000 Grenoble, France
5. Northern Rogue Studios, Oxford, UK
6. University of Chicago, 5801 S Ellis Ave, Chicago, IL 60637, United States
7. School of Engineering and Material Science, Queen Mary University of London, London
8. Section Palaeontology, Institute of Geosciences, Rheinische Friedrich-Wilhelms-Universität Bonn, Bonn, Germany

*e.panciroli@nms.ac.uk

Abstract

Living mammal groups exhibit rapid juvenile growth with a cessation of growth in adulthood[1]. Understanding the emergence of this pattern in the earliest mammaliaforms (mammals and their closest extinct relatives) is hindered by a paucity of fossils representing juvenile individuals. We report exceptionally complete juvenile and adult specimens of the Middle Jurassic docodontan *Krusatodon*, providing anatomical data and unprecedented insights into the life history of early-diverging mammaliaforms. We used synchrotron X-ray micro CT imaging of cementum growth increments within the teeth[2,3] to provide the first evidence of pace of life in a Mesozoic mammaliaform. The adult was ~7 years and the juvenile 7 to 24 months of age at death, and in the process of replacing its deciduous dentition with its final, adult generation. When analysed against a dataset of life history parameters for extant mammals[4], the relative sequence of adult tooth eruption was already established in *Krusatodon*, and within the range observed in extant mammals, but this development was prolonged; taking place during a longer period as part of a significantly longer maximum lifespan than extant mammals of comparable adult body mass (≤156 grams). Our findings suggest early-diverging mammaliaforms did not experience the same life histories as extant small-bodied mammals, and the fundamental shift to faster growth over a shorter lifespan may not have taken place in mammaliaforms until during or after the Middle Jurassic.

Introductory Paragraph

Understanding the origin and evolution of mammalian life history traits is a central aim of mammal palaeontology. Among living mammals, species with smaller adult body mass generally develop quickly, mature younger, live shorter lives and have larger litters than those with larger body masses[1]. The immediate predecessors of mammals (Mammaliaformes, the group that

includes Mammalia and their closest extinct relatives) had very small adult body masses (<100g [5,6]) and were at least moderately endothermic[7], but also exhibited longer life spans and slower growth rates[8,9] than small-bodied mammals of today. A paucity of fossil material of juveniles among early-diverging mammaliaforms limits our understanding of early ontogenetic growth in these animals, and the macroevolution of life history traits along the mammalian stem lineage.

We report partial skeletons of a juvenile (~40% complete) and adult (>95% complete) docodontan mammaliaform *Krusatodon kirtlingtonensis*, from the Bathonian Kilmaluag Formation (~166 Ma), at the Elgol Coast Site of Special Scientific Interest (SSSI), Isle of Skye, Scotland (Figures 1-3)[10,11]. Propagation phase-contrast synchrotron radiation X-ray micro-computed tomography (PPC-SRμCT) of circum-annually deposited increments preserved in dental cementum (Figures 3-4) reveals a prolonged early development in *Krusatodon* compared to modern mammals of similar adult body mass (≤156 g), with delayed dental eruption more similar to that of slow-growing extant mammals with larger body masses and longer maximum life spans (Figure 5). Nevertheless, the timing and sequence of eruption of adult teeth (related to weaning) relative to mandible length (a proxy for body size) is proportional to that of similar-sized extant mammals. This suggests that the ancestral blueprint of mammal growth had emerged by the Middle Jurassic, but that this growth took place over a prolonged time period due to slower growth rates, as evidenced by cementochronology.

Main Text

Overview

Mammals today comprise ~6,400 species[12] in three major clades, and exhibit a diverse range of life histories and developmental patterns. The earliest-diverging (~180-160 Ma) clade, the monotremes, are long-lived (22-50 years) and oviparous, laying small eggs (17 mm[13]) that hatch highly altricial neonates that develop relatively quickly. For example, *Ornithorhynchus* young can attain ~70% of their adult body mass by ~155 days old, when they emerge from the burrow[14,15] (Supplementary Table 1). Placental mammal young are born relatively precocial compared to monotremes and marsupials[16,17], which may have facilitated their impressive ecological diversity and wide range of locomotor abilities[18,19].

The growth and metabolic strategies of extant mammals are distributed along a so-called 'fast-slow' continuum[1,20,21,22,23,24]. Larger adult body mass is associated with slower mass-specific growth rates, lower mass-specific metabolic rates, longer lifespans, delayed sexual maturity, and the production of fewer, larger offspring with respect to adult mass[22,23]. This fast-slow pattern also appears to persist even when body mass and phylogeny are accounted for[24,25] and covaries partially with precociality and other ecological traits[23,26,27,28,29].

Most extant mammals exhibit determinate growth, reaching adult size proportionally early in their lives, followed by a cessation of growth[8] – although there are some exceptions, e.g. tenrecs and hyracoids[4]. Determinate growth is linked to the termination of skull growth in early ontogeny, which usually coincides with the eruption of the ultimate molar in extant mammals[30,31]. Mammal neonates must continue to feed during a considerable growth in size. To achieve this while maintaining occlusion between upper and lower teeth, eutherians form deciduous teeth in utero that generally erupt around the time of birth in precocial taxa, and afterwards in altricial ones[32]. Metatherians (the group that includes marsupials) develop incisors, canines and most premolars early in development, without replacement[33]. Only the third premolar is replaced during postnatal development, a derived pattern established early in the metatherian lineage[33,34].

Early-diverging mammaliaforms such as docodontans were diphyodont, with tooth replacement taking place postnatally[31,35]. Smith (2000) proposed that the 'primitive' sequence of replacement in ancestral eutherians comprised the eruption of all molars before the premolar tooth replacement was completed (a similar pattern to fast-growing, small-bodied modern placentals). However, in more ancient Mesozoic mammaliaforms (a more inclusive clade of fossil predecessors to crown Mammalia, of which eutherians are a subclade), new and rapidly expanding evidence shows the addition of posterior molars and continued growth of the dentary in docodontans and morganucodontans, indicating that their skulls experienced prolonged growth in later life stages[31,36,37,38]. The late addition of molars in a dentary that continues to grow is now also known in stem therians such as spalacotheriids and dryolestids[38]. This suggests that prolonged growth is the ancestral condition in early-diverging mammaliaforms and some mammals. Charting the emergence of determinate growth, as seen in the wide majority of extant mammals spanning the fast-slow growth continuum, and assessing how this growth is related to tooth replacement in Mesozoic mammaliaforms such as docodontans, is fundamental to our understanding of mammal evolutionary history as a whole.

Description

The specimens NMS G.1992.47.122.1 (adult) and NMS G.2023.8.1 (juvenile) were visualised using micro-computed tomography, and propagation phase-contrast synchrotron X-ray computed micro-tomography (PPC-SRμCT) (Table 1). They are identified as *Krusatodon kirtlingtonensis* based on dental morphology (Extended Data Figure 1; Supplementary). The skulls of both the adult and the juvenile are compressed in fossilisation, but their elements remain close to their original positions (Figure 1b-c, 2b and 3a-b). The anterior end of the left dentary of NMS G.1992.47.122.1 (NMS G.1992.47.124) is detached from the rest of the skeleton, and was visualised separately (Table 1) and used in reconstructions (Figure 1e, 3b and d). The dental formula for *Krusatodon* is 4.1.4.4 / 4.1.4.4, but the adult NMS G.1992.47.122.1 exhibits the pathological retention of the left p2, so the premolar count is five on the left dentary (Extended Data Figure 3c and f).

The juvenile NMS G.2023.8.1 is at an early growth stage, as indicated by the partial eruption of the permanent generation of dentition (Figure 4a-b; Extended Data Figure 2h and 4-5; Supplementary). The lower i2, i4, p1 and p3 are represented by their permanent generation. In the upper dentition, the I3 appears to be represented by the permanent generation. The first two molars are erupted in the upper and lower dentition, with the m3/M3 in the process of erupting. The remaining dentition are either first generation deciduous teeth, with their erupting successors within the alveoli (lower di1, di3, dc, and dp4, and dp5; upper dI1, dI2, dI4, dP1, dP2, dP3, dP5), or their generational assignment is unclear, mostly due to damage (p1, I3, C). The dp2 does not have a successor within the dentary, as this tooth is lost during the eruption of permanent dentition, as in *Haldanodon*[39]. This results in a lower premolar count in the adult animal compared to the juvenile (Extended Data Figure 2-5; Supplementary). This pattern of premolar loss occurs in the upper premolars as well, but breakage at this area in the juvenile fossil hinders interpretation. The p4 is in the process of erupting, the P4 does not appear to have a successor, and cementum suggests it is the deciduous generation, and the m4/M4 crypts are present, but m4/M4 has not formed. The coronoid process is laterally offset to the successively erupting molars, another indication that NMS G.2023.8.1 represents an early developmental stage[36].

In the adult NMS G.1992.47.122.1, the full permanent dentition is present including the fully erupted m4/M4, which in the extant opossums *Monodelphis* and *Caluromys* occurs when the animal is relatively old[32,40], supporting our interpretation that NMS G.1992.47.122.1 is a mature adult. Similarly, the coronoid process is in line with the tooth row and shifted posteriorly relative to the ultimate molar (Extended Data Figure 3a-f). This posterior shift continues through ontogeny in docodontans, indicating that the adult specimen is a senescent individual[36]. The Meckel's sulcus is closed ventral to m2/m3, after which it forms a faint indent that does not reach the ventral edge of the dentary, another feature indicative of maturity[36,41].

The high-resolution tomography of these exceptionally well preserved individuals of *Krusatodon kirtlingtonensis* provides several novel observations that are relevant to documenting evolutionary changes in the mammal stem. The external nares in *Krusatodon* are formed anteriorly and anteroventrally by the premaxilla, dorsally by the nasal, and posteriorly and posteroventrally by the septomaxilla (Figure 3c; Extended Data Figure 2g; Supplementary). A dorsally pointed internarial process is preserved on the premaxillae in NMS G.2023.8.1. A ridge on the dorsolateral edge of the nasal indicates that this dorsolateral edge lay beneath the septomaxilla, premaxilla, and then maxilla. The septomaxilla is preserved on both sides of the juvenile, and comprises a long ventral shelf that overlaps the palatal process of the premaxilla, and a lateral (facial) plate that dorsally contacts the lateral edge of the nasal. The intranarial process protruding from the ventral shelf, and the septomaxillary canal tunneling through the shelf (as seen in *Thrinaxodon*) are absent in *Krusatodon*. But it is uncertain if a septomaxillary foramen (as exemplified by *Sinoconodon*) would be present on the lateral surface of rostrum, because the foramen is in the contact area between the septomaxilla and the premaxilla, and this contact is not fully preserved. The presence of the septomaxilla is a basal

characteristic for earlier mammaliaforms[42,43], lost in crown therians. In *Morganucodon*, a facet for the septomaxilla is present on the premaxilla (Kermack et al 1981: p7), and a similar indentation is present in *Krusatodon*.

The procoracoid is present in *Krusatodon*, a plesiomorphic trait shared with morganuocdontans, the haramiyidan *Maiopatagium*[44] and extant monotremes[45]. However, it is absent in other docodontans for which this part of the scapulacoracoid is known, including *Haldanodon*[46], *Borealestes*[47], *Agilodocodon*[48], *Docofossor*[49], and *Microdocodon*[50], and in therians (see Supplementary Material). Its presence in *Krusatodon* indicates that it was lost twice within mammaliaforms: once within Docodonta, and separately in derived stem-therians after their divergence from australosphenidans (Figure 3e and Extended Data Figure 8; Supplementary).

In the scapulacoracoid, the coracoid is approximately 69% of the length of the glenoid facet, and the glenoid suture lies just above the dorsoventral midpoint of the glenoid facet (Extended Data Figure 8d). The scapula has a trough-like infraspinous fossa, which is similar to that of *Tachyglossus* (echidna). In *Tachyglossus* this fossa is for the origination of the M. infraspinatus, permitting humeral external rotation[45]. The postscapular fossa (sensu Martin [2005:fig 3]) is present and well-developed in *Krusatodon*. This is the insertion for the teres major muscle in *Tachyglossus*[45], permitting humeral internal rotation and powerful flexion and retraction of the humerus to the scapula[46].

The humeral radial and ulnar condyles are slightly larger and more bulbous, and the distal humerus proportionally wider in the adult *Krusatodon* compared to the juvenile (Extended Data Figure 6g-h). This reflects the full development and ossification of this portion of the bone in the mature individual, and similar ontogenetic differences in limb bones have been observed in other docodontans (Martin 2005: p231).

The prominent distal tibial malleolus, and the medial concavity on the astragalus in which the tibial malleolus pivoted (Extended Data Figure 6n-p and7k-m) are specialised ankle structures of the docodontan clade[47,48,49,50]. They permit a foot posture associated with a sprawling hindlimb stance, allowing a wide range of hyperextension and eversion in the foot[47], similar to living monotremes, in contrast to therian mammals. Full description of the anatomy of *Krusatodon* can be found in the Supplementary.

Histology and Cementochronology

To determine chronological ages of the fossil individuals, we used PPC-SRμCT to visualise growth increments preserved in dental cementum surrounding the tooth roots (Figure 3g and 4; Methods; Extended Data Figure 9-10). Cementum is a mineralised dental tissue that is deposited in a circum-annual series of increments of alternating opacity in histological thin-section[2,3] and X-ray attenuation in tomographic data[9]. Each pair of light/dark increments represents approximately one year of growth in extant mammals, with increment pair counts used to estimate chronological lifespan[51]. Cementum can also be detected in deciduous teeth, and in

extant mammals is deposited in the same seasonal cycles as in permanent dentition, if the deciduous teeth are retained through a deposition cycle[52, 53].

PPC-SRμCT data reveals two dark cementum increments surrounded by two light increments are present in the deciduous teeth and first molar of the juvenile (e.g. Figure 4e and f; Supplementary), and a single dark cementum increment and light increment is present in the more recently erupted permanent teeth (Figure 4c and d; Supplementary). The two increment pairs in the deciduous dentition and the single pair in the more recently erupted dentition of the juvenile *Krusatodon* suggests this animal had passed through a minimum of one complete cycle of cementum deposition prior to the eruption of the permanent dentition, and a maximum of two. At least six cementum increment pairs in the adult *Krusatodon* NMS G.1992.47.122.1 (e.g. Figure 3g; Supplementary). These data suggest that *Krusatodon* could live to at least seven years of age, similar to the extended life spans reported for earlier mammaliaforms such as *Morganucodon*[6].

Although cementum deposition cycles are generally considered annual[49,50], there is some variation in the exact timing of the first increment relative to birth[52,53], depending on the timing of birth in relation to seasons of growth, which may occur at different points in time during a year in different regions, climates, and habitats. New data obtained here for *Procavia* and *Macroscelides* (Table 1; Supplementary), accompanied by a review of previous studies[53, 54,55,56], suggests a range of timings for the first cementum increment of the deciduous dentition between 7–24 months. This suggests a conservative estimate that juvenile (NMS G.2023.8.1) represents an individual at least seven months in age, but potentially as much as two years old.

Weaning and Development

Among extant mammals, most species have 40-60% of their full adult dentition by the time they reach ~95% of their adult dentary length[27], which is a proxy for size. To establish if *Krusatodon* grew in a similar pattern to living mammals, we used the methodology of Asher and Lehman (2008) to examine tooth development of the juvenile against its jaw length (~24 mm) as a proportion of adult jaw length (30 mm). We found that it represents an animal with 49% of the adult dentition erupted at 80% adult dentary length, which places it within the range seen for extant taxa[27] (Figure 5a), albeit within lower half of that range similar to some primates, tenrecs and tree shrews, but proportionally larger than most individuals of the marsupial *Didelphis* at the same stage of dental eruption. It is worth noting that Asher and Lehman's dataset is biased towards afrotherians, which are known to have delayed dental eruption relative to other mammal groups. However, of the specimens in this dataset with 40-59% tooth eruption – as shown in Figure 5a – only 9 (n=29) out of 20 (n=94) genera are afrotherians, the rest being canids (=Carnivora), didelphids, erinaceids, primates, and scandentids, which are all proportionally smaller (and usually younger) than afrotherians at a comparable tooth development stage (Asher and Lehman, 2008). The results suggest that the relationship between dental eruption and proportional growth in this mammaliaform is similar to that observed in some extant mammals.

Our body mass estimate for the adult *Krusatodon* NMS G.1992.47.122.1 is between 54 g (using the sum of humeral and femoral shaft circumference [HC+FC]; 95% prediction interval: 23.1 g – 127 g) and 156 g (using dentary length; 40.5 g – 598 g), and for the juvenile it is between 32 g (HC+FC; 13.8 g – 76 g; estimating femoral shaft circumference by assuming identical proportions to the adult) and 80 g (dentary; 22 g – 327 g) (see Methods and Supplementary). The juvenile therefore represents an animal between 51-59% the body mass of the adult.

Weaning is a key stage in the early ontogeny of all mammals, and its timing can be estimated from the proportion of the erupted adult teeth. We reviewed literature on timing of dental eruption and weaning and established a dataset of 81 living species for which timing of dental eruption and timing of weaning were available (Supplementary Table 1). We show that among living mammals, weaning is usually complete or long-complete by the time 46% of the adult dentition has erupted, as it had in the juvenile *Krusatodon* (Figure 5b). This includes members of small-bodied mammal groups such as erinaceomorphs and macroscelideans. Only a few exceptions were found among small-bodied species sampled, such as some soricomorphs, some marsupials and some rodents (Supplementary Table 1). If *Krusatodon* followed the developmental schedule seen in the majority of extant mammals, as inferred from the timing of its adult tooth eruption relative to jaw length (proxy for body size), then the juvenile *Krusatodon* (NMS G.2023.8.1) likely represents an animal close to weaning, or weaned.

We plotted the proportion (percentage) of adult body mass against days after birth for weaning-age individuals in 333 taxa in our extant mammal sample, plus *Krusatodon*. Here we show that relative growth in *Krusatodon* is slow, proportionally similar to larger-bodied extant mammals (Figure 5c). The closest datapoints to *Krusatodon* using the youngest age of 7 months (210 days) include marsupials such as the brush-tailed possum *Trichosurus vulpecula*, and placentals such as the barbary macaque *Macaca sylvanus,* which reach only 31% and 22% of adult body mass at weaning, much less than the estimate for *Krusatodon* of 51-59%. In a subset of data comprising only smaller-bodied mammals within the size range estimated for *Krusatodon* (≤156 g), all extant species have reached adult size, or are close to it, within the age range of the juvenile *Krusatodon* specimen, even at its youngest possible age as determined by cementum increments, of 7 months (Figure 5d). This indicates slow growth in *Krusatodon*, with age at weaning comparable to generally much larger mammals.

These results demonstrate that *Krusatodon* underwent a prolonged developmental schedule with late onset of permanent tooth eruption (in calendar days/years) compared to living mammals of similar body mass. Relative growth in *Krusatodon* was slow, and key life history events such as weaning likely occurred chronologically later than in small-bodied extant mammals.

Discussion

As a stem mammal, the mammaliaform *Krusatodon* provides evidence for the ancestral state for the mammal crown group. This is reflected by various traits

shared by *Krusatodon* and many other Jurassic non-mammalian mammaliaforms, including small body mass[3], diphyodonty[29], an extended life span[6], slower growth rates[5,6], and as shown here, a prolonged developmental schedule with a longer maximum lifespan.

Our results suggest that a fundamental shift in mammal development took place in the Middle Jurassic. The modern mammal-like sequence of dental eruption was already established in early-diverging mammaliaforms of the Mesozoic prior to the divergence of docodontans. This eruption sequence then underwent a timing change, shifting earlier by accelerated juvenile growth and a faster cessation of adult growth, in the later evolution of crown Mammalia, as seen in extant lineages. This unique analysis of juvenile vs. adult teeth of *Krusatodon* shows that docodontans lived longer than extant mammals of comparable body mass, similar to lifespans recorded for Late Triassic/Early Jurassic mammaliaforms in the study of fossil-based datasets of individual adult teeth.[6] This suggests that a shift in growth patterns took place among stem mammals no earlier than the Middle Jurassic by shortening of maximum lifespans in crown therians. Our findings here reveal first-hand data on body size growth from juvenile to adult, mapped on yearly chronology, and support a mosaic of emerging mammal traits appearing asynchronously through the Mesozoic at different loci across the cynodont-mammaliaform phylogeny.

Docodontans exhibit a more derived mode of tooth replacement than earlier mammaliaforms or non-mammalian cynodonts[29,37,57], and are an exemplar early-divergent clade and exhibiting crown mammal-like traits such as increased molar complexity[33] and ecomorphological diversity[57] before the origins of crown Mammalia. These traits are likely correlated, as evidenced by their coupled emergence in later stem therians[57]. The timing of dental eruption relative to body size (as opposed to mass) shown here in docodontans appears similar to crown mammals. Our results show that docodontans achieved their complex dentition and ecomorphological disparity despite a different life history profile of slower growth rates and a prolonged span of development.

The new observation that early mammaliaforms exhibited a prolonged developmental schedule and longer maximum life span makes sense in light of studies showing these variables are correlated in extant mammals, especially in those which have unexpectedly long life-span for their body mass, such as chiropterans and primates[58]. Hyraxes (*Procavia*) and extant monotremes provide the closest extant analogues for the life history of docodontans, albeit at larger maximum body sizes (3.6 kg and 1.25-7.5 kg, Supplementary Table 1) than those of the docodontans studied here. The hyrax has a life span of ~10 years, beginning tooth replacement at ~8 months and completing eruption by 5 years (50% of their lifespan)[56,59,60]. Dentition can't easily be used as a proxy for development in monotremes as they are edentulous, but for the weaning age against body mass, monotremes represent the closest datapoint to *Krusatodon* in our extant dataset. This suggests they may retain a more plesiomorphic developmental schedule, but this cannot be tested empirically due to the low diversity of living monotreme species.

Prolonged development in early mammaliaforms fits with Schultz's observation that in longer-lived, slower-growing placental species, ultimate molars erupt later in ontogeny, after the premolar replacement[61]. Known as 'Schultz's Rule', this pattern is believed to reflect specialisations for prolonged postnatal growth, and has been observed in many primates, carnivorans, ungulates and afrotherians[27,30, 61] (although see[62, 63]). The new juvenile fossil of *Krusatodon* demonstrates that docodontans conform to this pattern. This does not preclude determinate growth in *Krusatodon*; a reduction in cementum increment width observed in the adult specimen studied here could suggest that growth slowed through life (Figure 3g). This may have been more similar to the determinate growth found in the majority of extant squamates, which lack the rapid growth rates of juvenile mammals, but do reduce growth rates through life along a slower trend than mammals of comparable size[64]. Docodontans have much smaller body mass coupled with prolonged dental development and jaw growth, a combination of characteristics no longer seen in extant taxa. This may potentially be the ancestral state for mammals as a whole.

Why the developmental schedule of crown mammals might have shortened, or growth rates accelerated, relative to the prolonged schedules of docodontans and morganucodontans, is a question that is currently difficult to answer. One suggestion is that evolutionary increases in growth rates were coupled with increasing basal metabolic rates (BMRs) and the development of mammalian endothermy, and with an overall 'speeding up' of mammal life cycles. This may have facilitated the more energetically demanding ecologies such as swimming and gliding that emerged among Middle Jurassic taxa[57,65]. Exactly when, and how rapidly, mammalian levels of endothermy emerged is subject to debate. Recent studies suggest high levels of endothermy emerged in some mammaliamorph cynodonts as early as the Late Triassic, but with variation among clades[4]. This pre-dates the shortening of developmental schedule inferred for cladotherians. Basal metabolic rates have been shown to be decoupled from body temperature across crown mammal evolution[66], and remained at subendothermic levels in early mammaliaforms[6]. It is likely that docodontans, as exemplified by *Krusatodon,* exhibited lower endothermy and basal metabolic rates than other early mammaliaforms, consistent with previous studies[6]. Despite this, docodontans are known for their exceptional ecological diversity[57,63], which somewhat contradicts the proposed relationship between ecological diversity and endothermy[65]. It is ultimately clear that docodontan mammaliaforms did not experience the same physiological life histories as extant small-bodied mammals. Until more juvenile stem mammalians are discovered and studied, challenges remain in addressing the tempo and mode of changes in mammal developmental schedules in the Mesozoic.

Conclusions

The discovery of contemporaneous juvenile and adult specimens of *Krusatodon* has provided an unprecedented insight into the developmental schedule of an early mammaliaform. Aside from providing a host of novel morphological and anatomical data, non-destructive imaging using synchrotron and laboratory based X-ray micro CT have permitted digital reconstruction and histological analysis of dental

cementum growth increments in both specimens. Using these new data, we have demonstrated that the development sequence of extant mammals, namely eruption of adult teeth relative to jaw length, was already established in early mammaliaforms, but that this sequence of development was prolonged and took place across a significantly longer maximum lifespan than extant mammals of comparable body mass.

The shortening of developmental schedules, which are correlated with fully determinate growth in extant mammals, likely evolved later, after the divergence of crown Mammalia. Although the drivers of this change are difficult to pinpoint without a more comprehensive sampling of juvenile specimens from other Mesozoic mammaliaforms, this exceptional juvenile specimen of a Middle Jurassic docodontan provides insight into the evolution of the shortened growth schedule of diverse mammals today from their Jurassic predecessors.

Main references

1 Western, D. Size, life history and ecology in mammals. *African Journal of Ecology*, **17**, 185–204 (1979)

2 Lieberman, D. E. Life history variables preserved in dental cementum microstructure. *Science*, **261**, 1162–1164 (1993)

3 Klevezal, G. *Recording Structures of Mammals* (CRC Press, 1995)

4 Asher, R. J. & Lehmann, T. Dental eruption in afrotherian mammals. *BMC Biology*, **6,** 1–11 (2008)

5 Kemp, T. S. *The origin and evolution of mammals* (Oxford University Press, 2005)

6 Lautenschlager, S., Gill, P. G., Luo, Z.-X., Fagan, M. J. & Rayfield, E. J. The role of miniaturization in the evolution of the mammalian jaw and middle ear. *Nature*, **561**, 533–537 (2018)

7 Araújo, R., David, R., Benoit, J., Lungmus, J.K., Stoessel, A., Barrett, P. M., Maisano, J. A., Ekdale, E., Orliac, M., Luo, Z.-X. & Martinelli, A. G. Inner ear biomechanics reveals a Late Triassic origin for mammalian endothermy. *Nature*, **607**, 726–731 (2022)

8 O'Meara, R. N. & Asher, R. J. The evolution of growth patterns in mammalian versus nonmammalian cynodonts. *Paleobiology*, **42**, 439–464 (2016)

9 Newham, E., Gill, P. G., Brewer, P., Benton, M. J., Fernandez, V., Gostling, N. J., Haberthür, D., Jernvall, J., Kankaanpää, T., Kallonen, A. & Navarro, C. Reptile-like physiology in Early Jurassic stem-mammals. *Nature Communications*, **11**, 1–13 (2020)

10 Panciroli, E., Benson, R. B. J., Walsh, S., Butler, R. J., Castro, T. A., Jones, M. E. & Evans, S. E. Diverse vertebrate assemblage of the Kilmaluag Formation (Bathonian, Middle Jurassic) of Skye, Scotland. *Earth and Environmental Science Transactions of the Royal Society of Edinburgh*, **111**, 135–156 (2020)

11 Benson, R. B. J., Butler, R. J., Evans, S. E., Jones, M. E. H., Panciroli, E., Tałanda, M. & Walsh, S. 2023. Squamates, mammals, salamanders and other small tetrapods from the Middle Jurassic Kilmaluag Formation, Isle of Skye, Scotland. Mesozoic Terrestrial Ecosystems 2023 (Abstract).

12 Burgin, C. J., Colella, J. P., Kahn, P. L. & Upham, N. How many species of mammals are there? *Journal of Mammalogy*, **100**, 615–615 (2019)

13 Hughes, L. R. & Hall, L. S. Early development and embryology of the platypus. *Philosophical Transactions of the Royal Society of London. Series B: Biological Sciences*, **353**, 1101–1114 (1998)

14 Holland, N. & Jackson, S. M. Reproductive behaviour and food consumption associated with the captive breeding of platypus (*Ornithorhynchus anatinus*). *Journal of Zoology*, **256**, 279–288 (2002)

15 Thomas, J., Handasyde, K., Parrott, M. L. & Temple-Smith, P. The platypus nest: burrow structure and nesting behaviour in captivity. *Australian Journal of Zoology*, **65**, 347–356 (2018)

16 Lillegraven, J. A. Biological considerations of the marsupial-placental dichotomy. *Evolution*, 707–722 (1975)

17 Weaver, L. N., Fulghum, H. Z., Grossnickle, D. M., Brightly, W. H., Kulik, Z. T., Wilson Mantilla, G. P. & Whitney, M. R. Multituberculate mammals show evidence of a life history strategy similar to that of placentals, not marsupials. *The American Naturalist*, **200**, 383–400 (2022)

18 Goswami, A., Randau, M., Polly, P. D., Weisbecker, V., Bennett, C. V., Hautier, L. & Sánchez-Villagra, M. R. Do developmental constraints and high integration limit the evolution of the marsupial oral apparatus? *Integrative and Comparative Biology*, **56**, 404–415 (2016)

19 Kelly, E. M. & Sears, K. E. Limb specialization in living marsupial and eutherian mammals: constraints on mammalian limb evolution. *Journal of Mammalogy*, **92**, 1038–49 (2011)

20 Boyce, M. S. Restitution of r- and K-selection as a model of density-dependent natural selection. *Annual Review of Ecology and Systematics*, **15**, 427–447 (1984)

21 Calder, W. A. III. *Size, Function and Life History*. (Harvard University Press, 1984)

22 Harvey, P. H. & Purvis, A. in *Advanced Ecological Theory: Principles and Applications* (ed McGlade, J.) 232–248 (Blackwell Science, 1999)

23 Fisher, D. O., Owens, I. P. & Johnson, C. N. The ecological basis of life history variation in marsupials. *Ecology*, **82**, 3531–3540 (2001)

24 Dobson, F. S. & Oli, M. K. Fast and slow life histories of mammals. *Ecoscience*, **14**, 292–299 (2007)

25 Harvey, P. H., Read, A. F. & Promislow, D. E. L. (editors) Life history variation in placental mammals: unifying the data with theory. *Oxford Surveys in Evolutionary Biology*, **6**, 13–31 (1989)

26 Gaillard, J. M., Pontier, D., Allaine, D., Lebreton, J. D., Trouvilliez, J. & Clobert, J. An analysis of demographic tactics in birds and mammals. *Oikos*, 59–76 (1989)

27 Purvis, A. & Harvey, P. H. Mammal life-history evolution: a comparative test of Charnov's model. *Journal of Zoology*, **237**, 259–283 (1995)

28 Oli, M. K. & Dobson, F. S. The relative importance of life-history variables to population growth rate in mammals: Cole's prediction revisited. *The American Naturalist*, **161**, 422–440 (2003)

29 Oli, M. K. The fast–slow continuum and mammalian life-history patterns: an empirical evaluation. *Basic and Applied Ecology*, **5**, 449–463 (2004)

30 Pond, C. M. The significance of lactation in the evolution of mammals. *Evolution*, 177–199 (1977)

31 Luo, Z.-X., Kielan-Jaworowska, Z. & Cifelli, R. L. in *Fanfare for an Uncommon Paleontologist Festschrift in Honor of Dr. Malcolm C. McKenna* (eds Dawson, M. R. and Lillegraven, J. A.) *The Carnegie Museum of Natural History Bulletin* **36**, 159–175 (2004)

32 Smith, B. H. Schultz's rule and the evolution of tooth emergence and replacement patterns in primates and ungulates. *Development, function and evolution of teeth*, 212–227 (2000)

33 Cifelli, R. L., Rowe, T. B., Luckett, W. P., Banta, J., Reyes, R. & Howes, R. I. Fossil evidence for the origin of the marsupial pattern of tooth replacement. *Nature*, **379**, 715–718 (1996)

34 van Nievelt, A. F. H. & Smith, K.K. The significance of reduced functional tooth replacement in marsupial and placental mammals. *Paleobiology*, **31**, 324–346 (2005)

35 Luo, Z.-X. & Martin, T. Analysis of molar structure and phylogeny of docodont genera. *Bulletin of the Carnegie Museum of Natural History*, **39**, 27–47 (2007)

36 Schultz, J. A., Bhullar, B.-A. S. & Z.-X. Luo. Re-examination of the Jurassic mammaliaform *Docodon victor* by computed tomography and occlusal functional analysis. *Journal of Mammalian Evolution*, **26**, 9–38. (2019)

37 Panciroli, E., Benson, R. B. J., Fernandez, V., Butler, R. J., Fraser, N. C., Luo, Z.-X. & Walsh, S. New species of mammaliaform and the cranium of *Borealestes* (Mammaliformes: Docodonta) from the Middle Jurassic of the British Isles. *Zoological Journal of the Linnean Society*, **192**, 1323–1362 (2021)

38 Luo, Z.-X. & Martin, T. Mandibular and Dental Characteristics of the Late Jurassic Mammal *Henkelotherium guimarotae* (Paurodontidae, Dryolestida). *Paläontologische Zeitschrift*, 1–51 (2023)

39 Martin, T. & Schultz, J. A. Deciduous dentition, tooth replacement, and mandibular growth in the Late Jurassic docodontan *Haldanodon exspectatus* (Mammaliaformes). *Journal of Mammalian Evolution*, 1–25 (2023)

40 Astúa, D. & Leiner, N. O. Tooth eruption sequence and replacement pattern in woolly opossums, genus *Caluromys* (Didelphimorphia: Didelphidae). *Journal of Mammalogy*, **89**, 244–251 (2008)

41 Kermack, K. A., Mussett, F. & Rigney, H. W. The lower jaw of *Morganucodon*. *Zoological Journal of the Linnean Society*, **53**, 87–175 (1973)

42 Crompton, A. W. & Luo, Z. in *Mammal phylogeny: Mesozoic differentiation, multituberculates, monotremes, early therians, and marsupials* (eds Szalay, F. S. Novacek, M. J. McKenna, M. C.) 30–44 (Springer, 1993)

43 Kermack, K. A., Mussett, F. & Rigney, H. W. The skull of *Morganucodon*. *Zoological Journal of the Linnean Society*, **71**, 1–158 (1981)

44 Meng, Q.-J., Grossnickle, D. M., Liu, D., Zhang, Y.-G., Neander, A. I., Ji, Q. & Luo, Z.-X. New gliding mammaliaforms from the Jurassic. *Nature*, **548**, 291–296 (2017)

45 Regnault, S., Fahn-Lai, P., Norris, R.M. & Pierce, S. E. Shoulder muscle architecture in the echidna (Monotremata: *Tachyglossus aculeatus*) indicates conserved functional properties. *Journal of Mammalian Evolution*, **27**, (2020)

46 Martin, T. Postcranial anatomy of *Haldanodon exspectatus* (Mammalia, Docodonta) from the Late Jurassic (Kimmeridgian) of Portugal and its bearing for mammalian evolution. *Zoological Journal of the Linnean Society*, **145**, 219–248 (2005)

47 Panciroli, E., Benson, R. B. J., Fernandez, V., Butler, R. J., Fraser, N. C., Luo, Z.-X. & Walsh, S. Postcrania of *Borealestes* (Mammaliformes: Docodonta) and the emergence of ecomorphological diversity in early mammals. *Palaeontology*, 65, e12577 (2022)

48 Meng, Q. J., Ji, Q., Zhang, Y. G., Liu, D., Grossnickle, D. M. & Luo, Z.-X. An arboreal docodont from the Jurassic and mammaliaform ecological diversification. *Science*, **347**, 764–768 (2015)

49 Luo, Z.-X., Meng, Q.-J., Ji, Q., Liu, D., Zhang, Y.-G., Neander, A. I. Evolutionary development in basal mammaliaforms as revealed by a docodontan. *Science*, **347** 760–764 (2015)

50 Zhou, C.-F., Bhullar, B.-A. S., Neander, A. I., Martin, T. & Z.-X. Luo. New Jurassic mammaliaform sheds light on early evolution of mammal-like hyoid bones. *Science*, **365**, 276–279 (2019)

51 Naji, S., Colard, T., Blondiaux, J., Bertrand, B., d'Incau, E. & Bocquet-Appel, J.-P. Cementochronology, to cut or not to cut? *International Journal of Paleopathology*, **15**, 113–9 (2016)

52 Furseth, R. A microradiographic and electron microscopic study of the cementum of human deciduous teeth. *Acta Odontologica Scandinavica*, **25**, 613–646 (1967)

53 Grue, H. & Jensen, B. Review of the formation of incremental lines in tooth cementum of terrestrial mammals [age determination, game animal, variation, sex, reproductive cycle, climate, region, condition of the animal]. *Danish Review of Game Biology*, **11**, 1–48 (1979)

54 Crowe, D. M. The presence of annuli in bobcat tooth cementum layers. *The Journal of Wildlife Management*, 1330–1332 (1972)

55 Crowe, D. M. & Strickland, M. D. Dental annulation in the American badger. *Journal of Mammalogy*, **56**, 269–272 (1975)

56 Fairall, N. Growth and age determination in the hyrax *Procavia capensis*. *African Zoology*, **15**, 16–21 (1980)

57 Luo, Z.-X. Transformation and diversification in early mammal evolution. *Nature*, **450**, 1011–1019 (2007)

58 Magalhães, J. P. D., Costa, J. & Church, G. M. An analysis of the relationship between metabolism, developmental schedules, and longevity using phylogenetic independent contrasts. *The Journals of Gerontology Series A: Biological Sciences and Medical Sciences*, **62**, 149–160 (2007)

59 Steyn, D. & Hanks, J. Age determination and growth in the hyrax *Procavia capensis* (Mammalia: Procaviidae). *Journal of Zoology*, **201**, 247–257 (1983)

60 Asher, R. J., Gunnell, G. F., Seiffert, E. R., Pattinson, D., Tabuce, R., Hautier, L. & Sallam. H. M. Dental eruption and growth in Hyracoidea (Mammalia, Afrotheria). *Journal of Vertebrate Paleontology*, **37**, p.e1317638 (2017)

61 Schultz, A. H. in *Human Growth, vol. III* (ed. Tanner, J. M.) 1–20 (Pergamon Press, 1960)

62 Godfrey, L. R., Samonds, K. E., Wright, P. C. & King, S.J. Schultz's unruly rule: dental developmental sequences and schedules in small-bodied, folivorous lemurs. *Folia Primatologica*, **76**, 77–99 (2005)

63 Monson, T.A. and Hlusko, L.J., 2018. The evolution of dental eruption sequence in artiodactyls. *Journal of Mammalian Evolution*, **25**, 15–26.

64 Frýdlová, P., Mrzílková, J., Šeremeta, M., Křemen, J., Dudák, J., Žemlička, J., Minnich, B., Kverková, K., Němec, P., Zach, P. & D. Frynta. Determinate growth is predominant and likely ancestral in squamate reptiles. *Proceedings of Royal Society. B*, **287**, 20202737 (2020)

65 Newham, E., Gill, P. G. & Corfe, I. J. New tools suggest a middle Jurassic origin for mammalian endothermy: advances in state-of-the-art techniques uncover new insights on the evolutionary patterns of mammalian endothermy through time. *BioEssays*, **44**, 2100060 (2022)

66 Avaria-Llautureo, J., Hernández, C. E., Rodríguez-Serrano, E., & Venditti, C. The decoupled nature of basal metabolic rate and body temperature in endotherm evolution. *Nature*, ***572***, 651–654 (2019)

Tables

Table 1: List of parameters used for micro-computed tomography (microCT) acquisition of the specimens.

Specimen number	Description	CT system	Voxel size (µm)	N. of Proj.	Filter	kV	µA	Exp. (s)	Fr. av.
NMS G.1992.47.122.1	*Krusatodon kirtlingtonensis* - near complete skeleton of fully grown adult	ESRF	13	6000	5.6mm Al; 1.4mm Cu; 1mm W	190	na	0.1	10
NMS G.1992.47.124 (whole)	*K. kirtlingtonensis* - anterior tip of the left dentary, part of NMS G.1992.47.122.1	Nikon XTH 225 ST (UoB)	12.78	3141	-	120	110	-	-
NMS G.1992.47.124 (cementum)	*K. kirtlingtonensis* - anterior tip of the left dentary, part of NMS G.1992.47.122.1	SLS	0.478	5001	100µm Al; 40µm Cu; 10µm Fe	30	-	0.22	-
NMS G.2023.8.1 – part A (whole)	*K. kirtlingtonensis* - posterior and central parts of the skull plus various postcrania	Nikon XTEK H 225 ST (Cam)	10.34	3142	-	170	155	1	4
NMS G.2023.8.1 – part A (cementum)	*K. kirtlingtonensis* - posterior and central parts of the skull plus various postcrania	SLS	0.478	5001	100µm Al; 40µm Cu; 10µm Fe	30	-	0.22	-
NMS G.2023.8.1 – part B (whole)	*K. kirtlingtonensis* - anterior part of the skull	Nikon XTEK H 225 ST (Cam)	15	2000	-	170	120	0.71	1
NMS G.2023.8.1 – part B (cementum)	*K. kirtlingtonensis* - anterior part of the skull	SLS	0.478	5001	100µm Al; 40µm Cu; 10µm Fe	30	-	0.22	-
NMS G.2023.8.1 – part C	*K. kirtlingtonensis* – bone scraps only	Nikon XTEK H 225 ST (Cam)	13.6	3142	-	170	120	0.71	2
NHMUK M.46526	*K. kirtlingtonensis* - right lower molar	Zeiss Xradia 520 Versa (NHMUK)	5.99	2401	LE4	110	90.9	1	-
NMS GH101.10 (cementum)	*Procavia*	SLS	0.478	2501	100µm Al; 40µm Cu; 10µm Fe	30	-	0.22	-
W11, W12 and W30 (cementum)	*Macroscelides*	SLS	0.325	2501	100µm Al; 10µm Fe	30	-	0.22	-

N. of Proj = number of projections; fr. av. = frame averaging; Cam = University of Cambridge; ESRF = European Synchrotron Radiation Facility; NHMUK = Natural History Museum, London; SLS = Swiss Light Source; UoB = University of Bristol. For ESRF parameters, the voltage column (kV) indicates the detected total integrated energy in keV.

Figure Legends

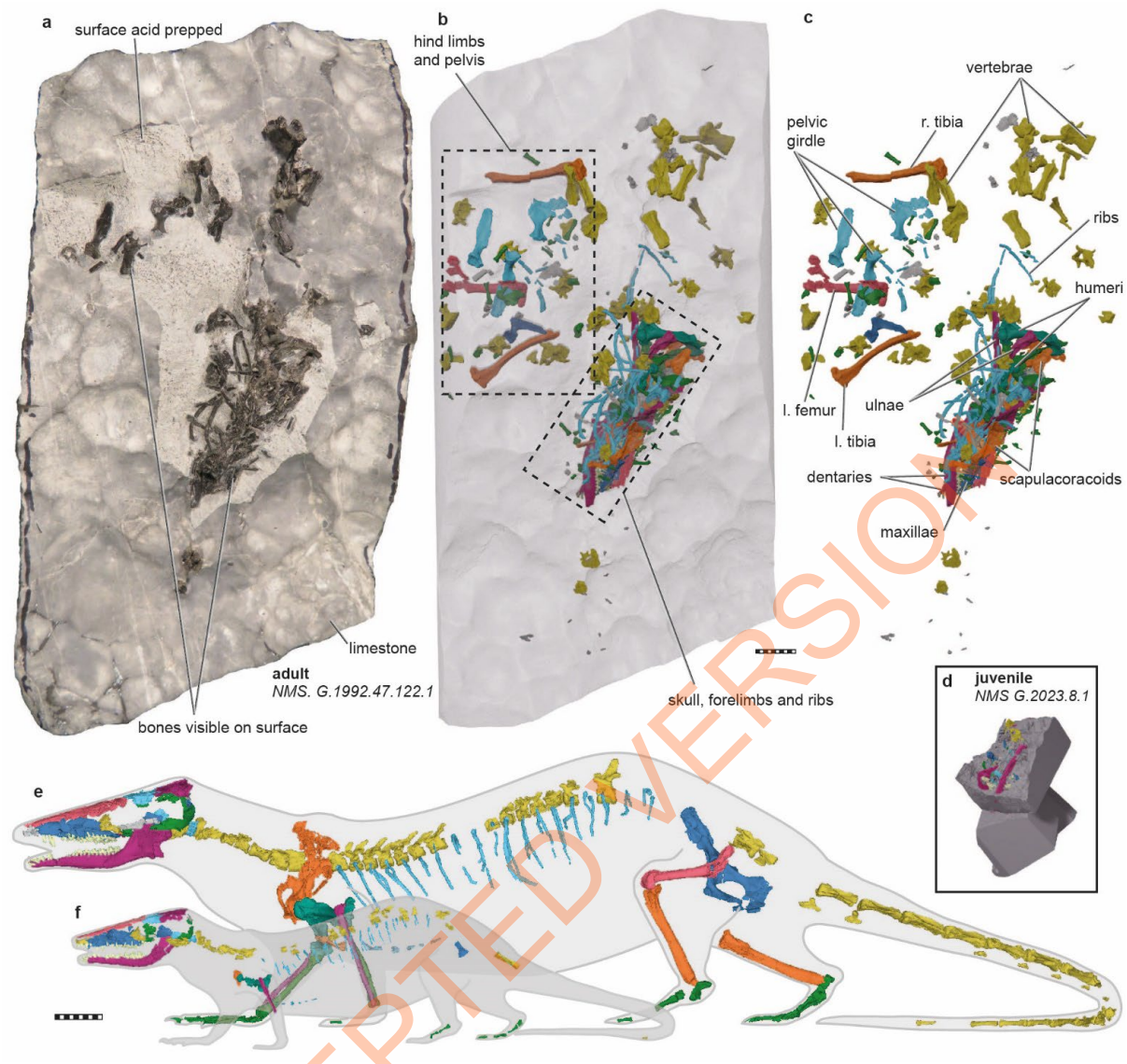

Figure 1: New specimens of *Krusatodon kirtlingtonensis*. **a**, photograph of adult NMS. G.1992.47.122.1 as preserved; **b**, cropped digital render of NMS. G.1992.47.122.1 showing contents; **c**, digital rendering of NMS. G.1992.47.122.1 with labelled skeletal elements; **d**, digital rendering of juvenile NMS G.2023.8.1 to same scale; **e**, reconstruction of preserved skeletal elements of adult NMS. G.1992.47.122.1; **f**, reconstruction of preserved skeletal elements of juvenile NMS G.2023.8.1. Scale bar same for a-d, and for e-f = 10 mm.

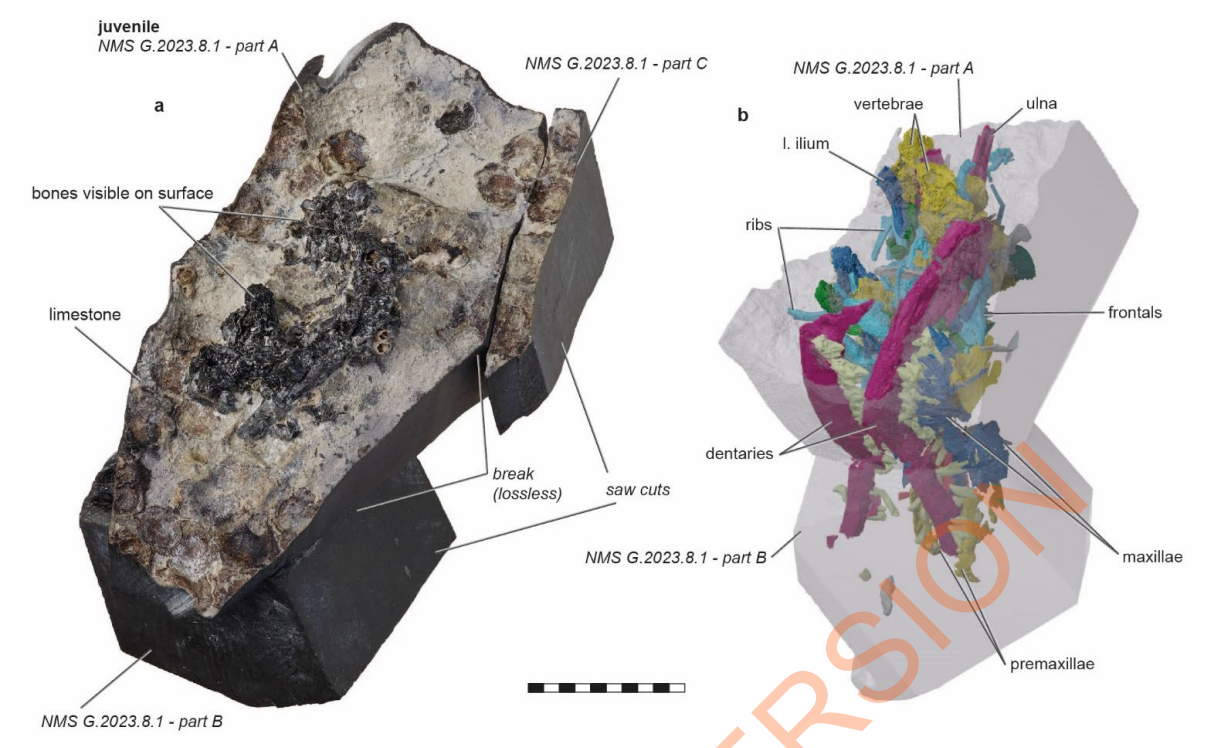

Figure 2: Juvenile specimen of *Krusatodon kirtlingtonensis*, NMS G.2023.8.1. **a**, photograph of NMS G.2023.8.1; **b**, cropped digital rendering of parts A and B of NMS G.2023.8.1 showing contents. Scale same for a-b. Scale bar = 10 mm.

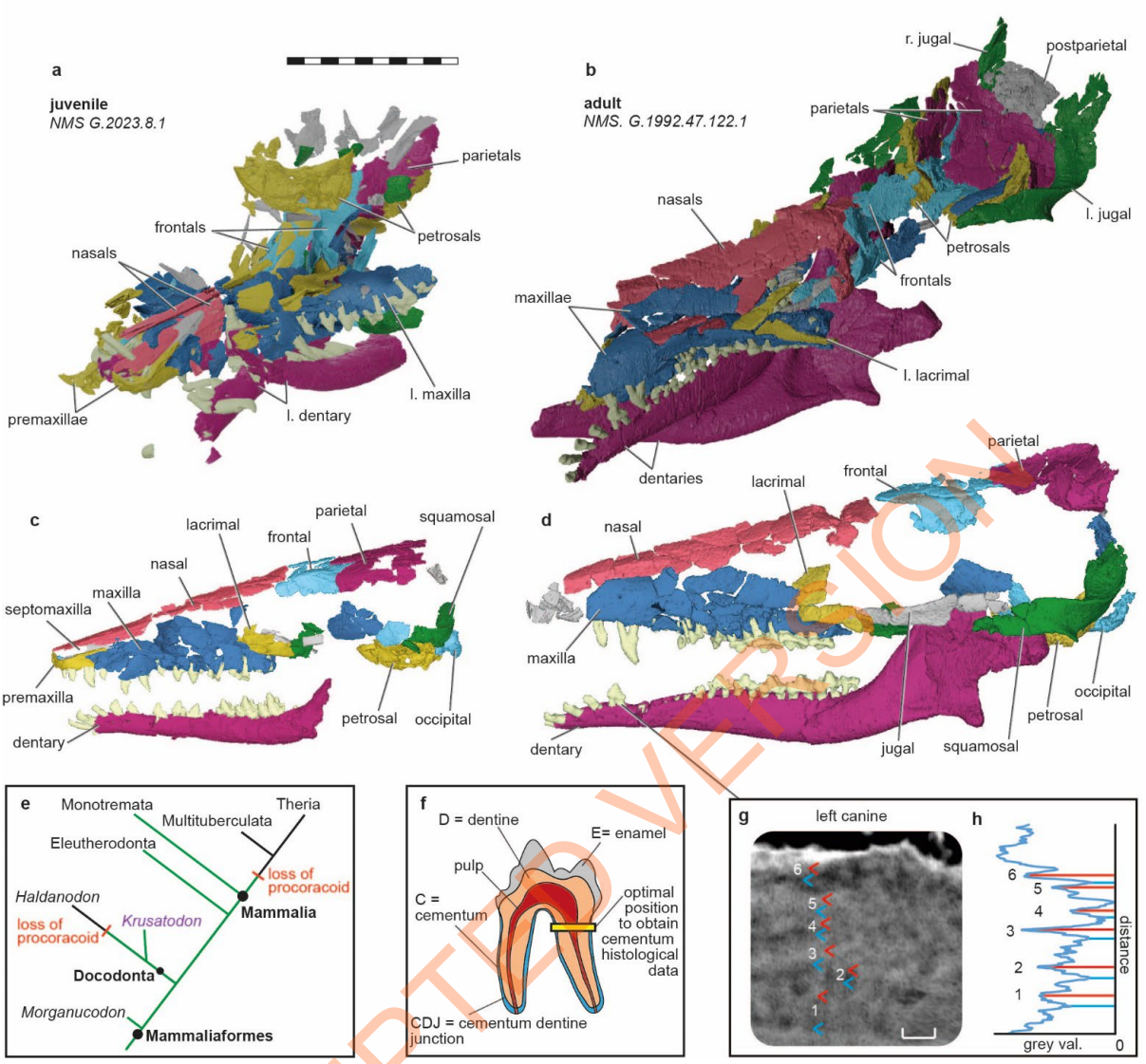

Figure 3: Juvenile and adult skulls of *Krusatodon kirtlingtonensis*, overview of phylogeny, and cementum for adult. **a**, digital rendering of the skull of juvenile NMS G.2023.8.1 as preserved; **b**, digital rendering of skull of adult NMS. G.1992.47.122.1, as preserved; **c**, reconstruction of preserved skull of NMS G.2023.8.1; **d**, reconstruction of preserved skull of NMS. G.1992.47.122.1; **e**, simplified phylogeny showing placement of docodontans, and loss of procoracoid; **f**, diagrammatic cross section of a molar; **g-h**, histological cross sections of cementum in tooth roots of canine in NMS. G.1992.47.122.1, and histogram of greyscale values for cross section (cross sections taken 4 times with similar results). Scale same for a-d, scale bar = 10 mm. Scale bar for g = 0.001 mm.

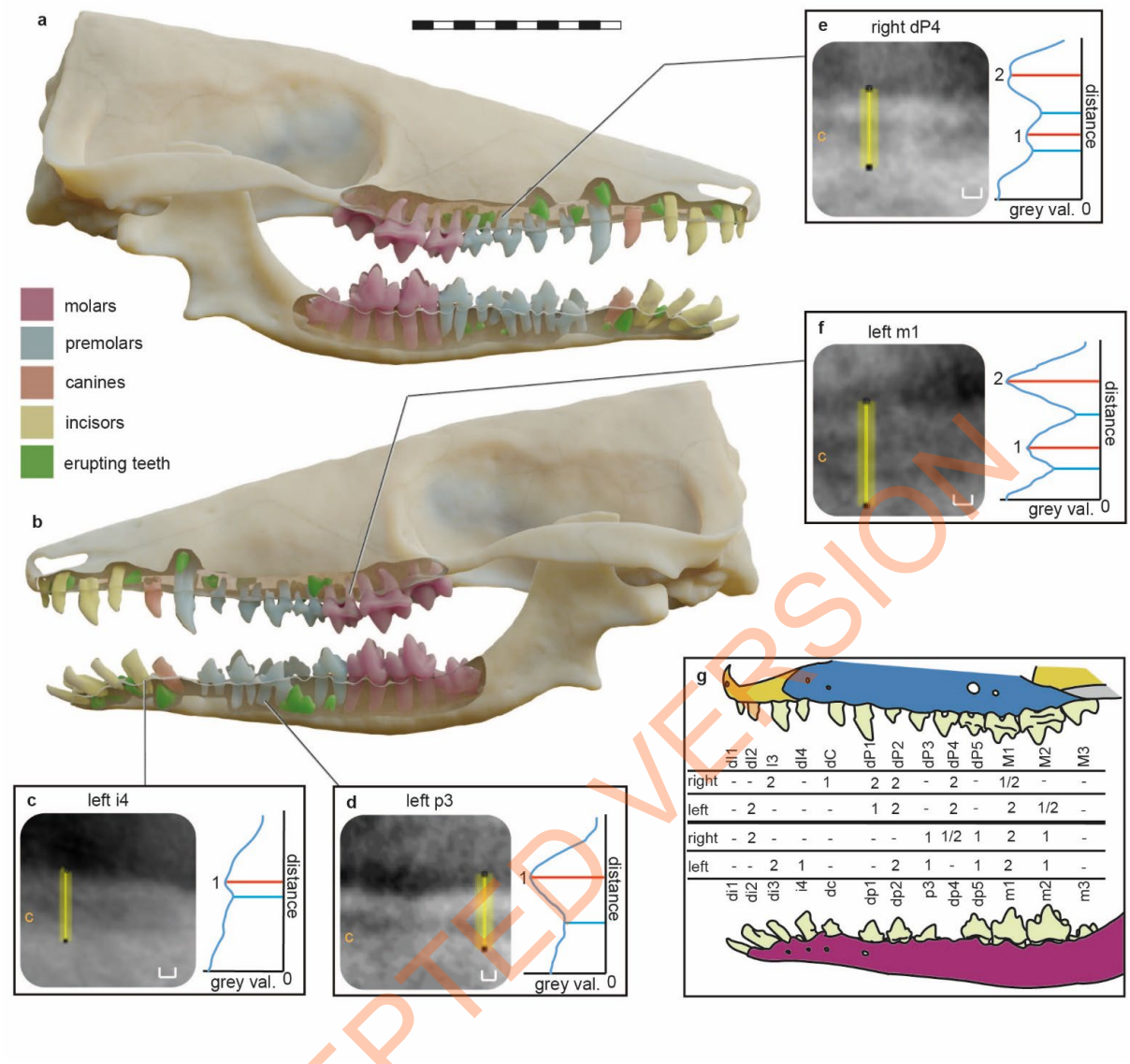

Figure 4: Reconstructed skull and cementum chronology for juvenile *Krusatodon kirtlingtonensis,* NMS G.2023.8.1. **a**, right lateral view of reconstructed skull showing cross section of tooth rows with erupting teeth; **b**, left lateral view of reconstructed skull showing cross section of tooth rows with erupting teeth; **c-f**, histological cross sections of cementum in tooth roots of NMS G.2023.8.1, and histogram of greyscale values for cross section (as indicated in cross section by yellow line), locations of cross sections in tooth row indicated in **a-b,** (cross sections taken 4 times with similar results); **g**, summary of tooth cementum increment pair counts for juvenile NMS G.2023.8.1 (lower teeth on bottom two rows, upper teeth on upper two rows). Scale bars for a-b = 10 mm; for **c-f** = ~0.01 mm.

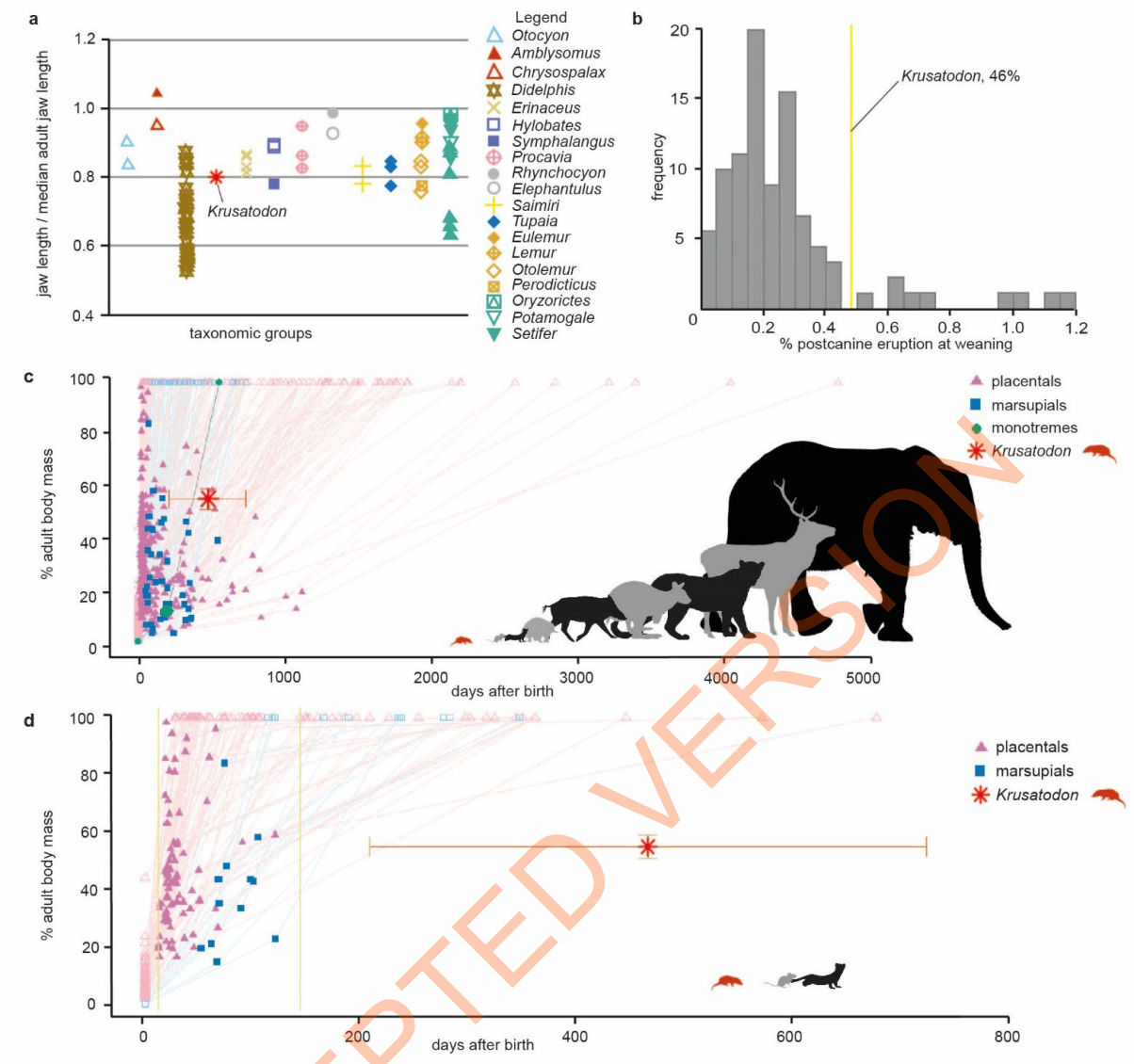

Figure 5: Analyses of body size and mass against tooth eruption and weaning time. **a**, extant mammal body size as a proportion of jaw length in mammals with 40-59% of 'cheek teeth' erupted, against final adult jaw length, data from Asher and Lehman (2008) with addition of *Krusatodon* NMS G.2023.8.1. Data points represent individual specimens within each genus (n=123); **b**, extant mammal percentage of postcanine tooth eruption at weaning, yellow line represents percentage eruption for *Krusatodon*; **c**, extant mammal body mass at birth, weaning, and adulthood, as a percentage of adult mass, against time in days (n=334). Red error bars represent range of estimated body mass (51-59% of adult body mass) and age (210-730 days) for juvenile *Krusatodon* NMS G.2023.8.1. **d**, as for c, but only including extant mammals ≤156 g (=max. estimate for adult *Krusatodon*), plus *Krusatodon* NMS G.2023.8.1 (n=97). Vertical yellow line represents last postcanine dental eruption in dataset for extant mammals in this size range. Silhouettes: adapted from Phylopic [https://creativecommons.org/licenses/by/3.0/].

Methods

Laboratory X-ray Micro-Computed Tomography

Details of scan parameters can be found in Table 1. NMS G.1992.47.124 (adult dentary tip) was imaged using laboratory-based computed tomography on a Nikon XTH 225 ST at the University of Bristol. NMS G.2023.8.1 (juvenile) was imaged using laboratory-based computed tomography on a Nikon XTEK H 225 ST micro-CT scanner at Cambridge Biotomography Centre, University of Cambridge. NHMUK M 46526 was imaged using laboratory-based computed tomography on a Zeiss Xradia 520 Versa at the Natural History Museum, London UK, with source object distance 19 mm, object detector distance 200 mm, optical magnification 0.39x, camera binning 2x2. All digital reconstructions were carried out using Materialise Mimics 19.0.

Propagation Phase-Contrast Synchrotron Radiation X-ray Micro-Computed Tomography

Details of scan parameters can be found in Table 1. NMS G.1992.47.122.1 was imaged at the ID19 beamline of the European Synchrotron Radiation Facility (Grenoble, France). The experimental setup consisted of: white beam from a wiggler (W150B gap 26.5 mm), indirect detector comprising a 500 µm LuAG scintillator, a set of 2 Hasselblad lenses (HC 2.2/100 mm and HC 4/210 mm (Victor Hasselblad AB, Gothenburg, Sweden) resulting in a 0.48x magnification, and a PCO.edge 5.5 sCMOS (PCO, Kelheim, Germany); sample-detector distance of 9 m for propagation phase contrast. Acquisition parameters: 6000 projections over a continuous rotation of 360°, integration time per projection of 0.1 sec (accumulation of 10 frames of 0.01 sec).The protocol to circumvent the limited size of the image (h x v: 688 x 2208 pixels = 8.94 x 28.70 mm) was: 1) performing several acquisition along the vertical axis, allowing to stack resulting tomograms (movement during the vertical series of 4.46 mm between each acquisition, resulting in a 50% overlap between consecutive acquisition); 2) offset on the centre of rotation to increase the size of the reconstructed tomogram (offset of 13 mm corresponding to 1000 pixels on the detectors, resulting in tomograms of 4208 x 4208 pixels); 3) two adjacent vertical series were captured and merged during post-processing.

Pre-reconstruction processing: radiograph stitching followed the protocol described in Benoit et al. (2019). Tomographic reconstruction using PyHST2 with phase retrieval approach[67,68], generating tomogram in 32-bits; post-processing included: 32-bits to 16 bits conversion, using the same parameters for both vertical series, ring correction[69], and finally merging of the two vertical series using a weighted average on the overlapping part.

All digital reconstructions were carried out using Materialise Mimics 19.0.

NMS G.1992.47.124, NMS G.2023.8.1, *Procavia* NMS GH101.10, and *Macroscelides* W11, W12 and W30 were all imaged for histological analysis at the TOMCAT (TOmographic Microscopy and Coherent rAdiology experiments) beamline X02DA of the Swiss Light Source at the Paul Scherrer Institute (Villigen, Switzerland). A multi-scale imaging setup was used to obtain complete, lower

resolution scans at ~6.5 µm of the full specimens, and then target the roots of in-situ teeth for high-resolution imaging of cementum increment pairs at ~0.48 µm resolution. Data were obtained for each tooth in the complete tooth row of the juvenile specimen of *Krusatodon* and for the anterior dentition of the adult – the size of this specimen limited the data we could collect, restricting collection to this detached portion of the dentary (NMS G.1992.47.124).

Body Mass Estimation

Body mass for extant mammals used in life history estimates (Figure 5a-d) was derived from the literature, see Life History Calculations.

Two body mass estimation methods were used to estimate the mass of *Krusatodon* specimens based on analysis of a novel dataset of skeletal measurements and body mass for small-bodied mammal, described in the Supplementary. Dentary length (DL) was used in the formula:

$\log_{10}(\text{body mass[g]}) = 2.979 \times \log_{10}(\text{DL}) - 2.208$

This calculation is similar to the equation of Foster (2009)[70], which is applied widely in studies of fossil mammals, and has the benefit of being more easily applicable because the dentary is preferentially preserved in the fossil record. The dentary measurement was taken from the anteriormost point of the alveolar rim of i1, to the posteriormost point of the dentary in line with the dentary condyle. Docodontans have proportionally long dentaries (and crania) and proportionally short femora compared to body mass relative to those of crown mammals (Meng et al. 2015: sp11). We therefore expect body mass estimates based on dentary lengths to be and over-estimate of the body masses of docodonts, and use these values for two specific purposes: (i) As an upper-bound estimate of the adult body mass of *Krusatodon*, and (ii) As an independent validation of the relative body mass of the juvenile specimen of *Krusatodon* compared to the adult.

The second method used the sum of humeral minimum shaft circumference and femoral minimum shaft circumference (HC + FC), via the formula:

$\log_{10}(\text{body mass[g]}) = 2.595 \times \log_{10}(\text{HC+FC}) - 0.990$

This calculation is similar to the equation of Campione and Evans (2012)[71], but is calculated from a dataset of small-bodied mammals (< 1 kg; see Supplementary).

These results indicate:

NMS G.1992.47.122.1 (adult)

HC+FC: 54.1 g (95% prediction interval: 23.1 g – 127 g)

Dentary length: 156 g (95% prediction interval: 40.5 g – 598 g)

NMS G.2023.8.1 (juvenile)

HC+FC: 32.4 g (95% prediction interval: 13.8 g – 76.0 g)

Dentary length: 80.2 g (95% prediction interval: 22.3 g – 327 g)

This places the adult *Krusatodon* between the size range of pygmy tree shrews (*Tupaia* ~58 g) and degus (*Octodontomys* ~158 g). Dividing the juvenile estimate by the adult estimate, the juvenile represents an animal between 51-59% the body mass of the adult.

Histological Analysis

Histological sectioning was carried out using hi-resolution synchrotron tomography on NMS G.1992.47.124 and NMS G.2023.8.1. A sub-micron resolution is required to visualise layers of cementum, a mineralised dental tissue that is deposited in an annual series of alternating light and dark increments, particularly on the root proximal to the tooth crown[2,3,53,].

The orientation of scan data was changed to match the long-axis of the tooth/root using VGStudio Max, and the straightened datasets saved (Supplementary). A single image was captured from the dorsal most portion of the tooth root, below the tooth crown. Cementum counts were made by visually inspecting these images for an initial count, then using ImageJ to select and straighten the cementum-bearing tooth layers, and creating histograms of grey values. The peaks and troughs of this histogram were used – with reference to the source image – to count the cementum layers (if present). Difficulties tracing bands for long distances around the tooth can lead to small margins of error in cementum counts, which is a limitation of this method for age estimation, more often in older individuals with multiple increments (2+) in which increments can merge and split. This limitation is less relevant to this study, in which any presence of increments is significant in the juvenile, and fits within the margin of error used in our analysis.

Additional cementum increment data was also gathered from *Procavia* NMS GH101.10, and *Macroscelides* W11, W12 and W30, using the same procedure as above. For full datasets, table of results and images see Supplementary.

Life History Calculations

The dataset for calculations of birth mass, adult body mass and weaning age was compiled using the AnAge database (https://genomics.senescence.info/species/index.html), with additional data from the literature (for full list of references see notes in Supplementary Table 1). For age of maturity in days, data from Promislow and Harvey (1990)[72] were originally in years, so were multiplied by 365.

To explore weaning age in mammals we divided weaning age by dental eruption completion age (see Supplementary Table 1 for list of sources for dental eruption completion).

To examine dental development against body size, we used the dataset of Asher and Lehman (2008, Supplementary File 2 available from https://bmcbiol.biomedcentral.com/articles/10.1186/1741-7007-6-14#Sec10). The juvenile specimen of *Krusatodon* NMS G.2023.8.1 has four out of eight permanent

"cheek teeth" (postcanines) erupted (p1, p2, m1, m2). Therefore, it has a value of 5.00 in for the column 'erupted/10' of Asher and Lehman (2008), or 50% adult dental eruption. To compare its relative size, as a proportion of adult size (0.8 in NMS G.2023.8.1) to those of living mammals at a similar stage of dental eruption therefore, we plotted proportional size data ('prop_adultJaw' of Asher and Lehman 2008) for all specimens of living mammals with 40-59% of adult dental eruption (Figure 5a). The dataset of Asher & Lehman (2008) contained 1 carnivoran (n=2), 2 chrysochlorids (n=2), 1 didelphid (n=43), 1 erinaceid (n=4), 2 hominoids (n=3), 1 hyracoid (n=4), 2 macroscelids (n=2), 1 platyrrhine (n=2), 1 scandentid (n=4), 4 stepsirhinids (n=7), and 4 tenricids (n=21) in this category. All subsets and plots can be reproduced using the R-code in Supplementary Material.

Inclusion and Ethics Statement

This study was led by a local researcher (EP). Roles and responsibilities for co-authors were agreed prior to work commencing at each stage. Fieldwork was conducted in consultation with the landowners, John Muir Trust, and NatureScot, with full permissions obtained. Appropriate risk assessments were made for fieldwork.

Data Availability

The CT and PPC-SRμCT datasets generated and analysed in this study are available in the Morphosource repository: www.morphosource.org/projects/00000C428

Additional data including the cementum increments (images and histograms) and data for body mass scaling relationships are outlined in SI, and available for download from Figshare: https://doi.org/10.6084/m9.figshare.25341508

Code Availability

We use R code in R studio for our analyses, adapting existing packages and code. No new packages were developed for this study. R code scripts are included in the SI, and available for download from Figshare: https://doi.org/10.6084/m9.figshare.25341508

Methods References

67 Mirone, A., Brun, E., Gouillart, E., Tafforeau, P. & Kieffer, J. The PyHST2 hybrid distributed code for high speed tomographic reconstruction with iterative reconstruction and a priori knowledge capabilities. *Nuclear Instruments and Methods in Physics Research Section B: Beam Interactions with Materials and Atoms*, **324**, 41–48 (2014)

68 Paganin, D., Mayo, S. C., Gureyev, T. E., Miller, P. R. & Wilkins, S. W. Simultaneous phase and amplitude extraction from a single defocused image of a homogeneous object. *Journal of Microscopy*, **206**, 33–40 (2002)

69 Lyckegaard, A., Johnson, G. & Tafforeau, P. Correction of ring artifacts in X-ray tomographic images. *International Journal of Tomography and Statistics*, **18**, 1–9 (2011)

70 Foster, J. R. Preliminary body mass estimates for mammalian genera of the Morrison Formation (Upper Jurassic, North America). *PaleoBios*, **28**, 114–122 (2009)

71 Campione, N. E. & Evans, D.C., A universal scaling relationship between body mass and proximal limb bone dimensions in quadrupedal terrestrial tetrapods. *BMC Biology*, **10**, 1–22 (2012)

72 Promislow, D. E. & Harvey, P.H. Living fast and dying young: A comparative analysis of life-history variation among mammals. *Journal of Zoology*, **220**, 417–437 (1990)

Acknowledgements
EP was funded by the Leverhulme Trust, the University of Oxford's John Fell Fund, and Linacre College's EPA Cephalosporin Fellowship. Some of the scans of NMS G.1992.47.124 and NMS G.1992.47.122.1 were undertaken while EP was funded by the Natural Environment Research Council (NE/L002558/1). Thanks to Ketura Smithson and Tom Davies for assistance with CT scanning, and to Elizabeth Griffiths, Alberto-Martin Serra and Stephanie Wright for segmenting scan data of extant mammal limb bones. Thanks to Robert Asher, Yves Candela, Mike Day, Zena Timmons for loan of specimens. Thanks to Tom Davies, Nuria Melisa Morales García, Pam Gill, and Julia Schultz for their assistance obtaining scan data. We acknowledge the European Synchrotron Radiation Facility (ESRF) and the Swiss Light Source at the Paul Scherrer Institute for provision of synchrotron radiation facilities and we would like to thank the beamline staff for assistance and support in using beamline ID19 (ESRF proposal ES587) and TOMCAT (proposal 20182126). We are grateful to Neil Brocklehurst for assistance with R coding. We would like to thank NatureScot and the John Muir Trust for permission to work on the Elgol Coast SSSI and NCO, and the fieldwork teams for their work. All fieldwork has been carried out in adherence to The Scottish Fossil Code.

Author contributions
E.P. was principle investigator. E.P., R.B.J.B., S.W., N.F and Z-X.L. contributed to the conception and design of overall project. E.P., R.B.J.B., and E.N. contributed to design of methodology. S.W. and N.F. provided access to specimens and logistical support. E.P., R.B.J.B., and S.W carried out fieldwork. E.P., R.B.J.B., V.F., E.N. and S.W. collected micro CT and synchrotron CT data. E.P. carried out digital segmentation, data collection, and histological analysis, and life history calculations. E.N. carried out additional cementum analysis. R.B.J.B. carried out body mass

calculations. E.P. and M.H. carried out digital reconstruction, visualisation, and figure preparation. E.P. led manuscript preparation and writing, and all authors contributed to editing the manuscript.

Competing interests
The authors declare no competing interests.

Materials & Correspondence
Correspondence and requests for materials should be addressed to Dr Elsa Panciroli - elsa.panciroli@oum.ox.ac.uk

Supplementary
The file includes a section on body mass estimates, systematic palaeontology, an extended osteological description, phylogenetic analysis and results, information on the procoracoid, further information on the cementochronology data, R code and supplementary references.

Extended Data Figures

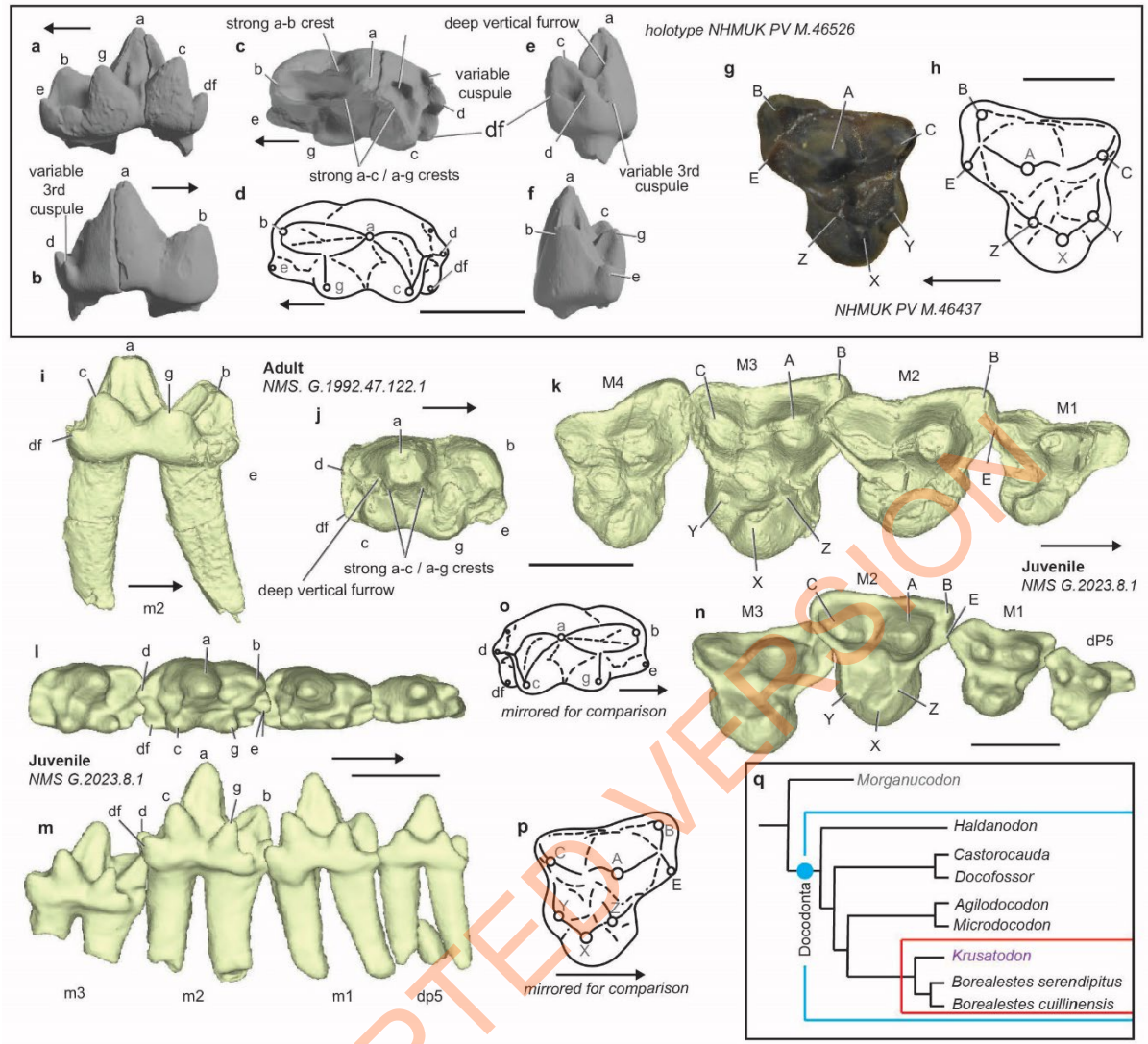

Extended Data Figure 1: Molar morphology in *Krusatodon kirtlingtonensis*. All digital renderings except for diagrammatic outlines and **g** (photograph). **a-f**, holotype lower right molar NHMUK PV M.46526 in: **a**, lingual; **b**, labial; **c**, occlusal; **d**, diagrammatic occlusal; **e**, posterior; **f**, anterior view. **g-h** NHMUK PV M.46437 upper left molar (M3) in: **g**, occlusal; **h** diagrammatic occlusal views. **i-k**, adult NMS. G.1992.47.122.1: **l**, lower m2 in lingual view; **j**, and occlusal view; **k**, upper molar row occlusal view. **l-n**, juvenile NMS G.2023.8.1: **l**, lower left molar tooth row plus dp5 occlusal view; **m**, and lingual view. **n**, upper right molar tooth row plus dP5 in occlusal view. **o-p**, mirrored versions of D and H to facilitate comparison. **q**, results of phylogenetic analysis for Docodonta including new scores for *Krusatodon*. **a-f** same scale, **g-h** same scale, **i-k** same scale, **l-n** same scale. All scale bars = 1 mm.

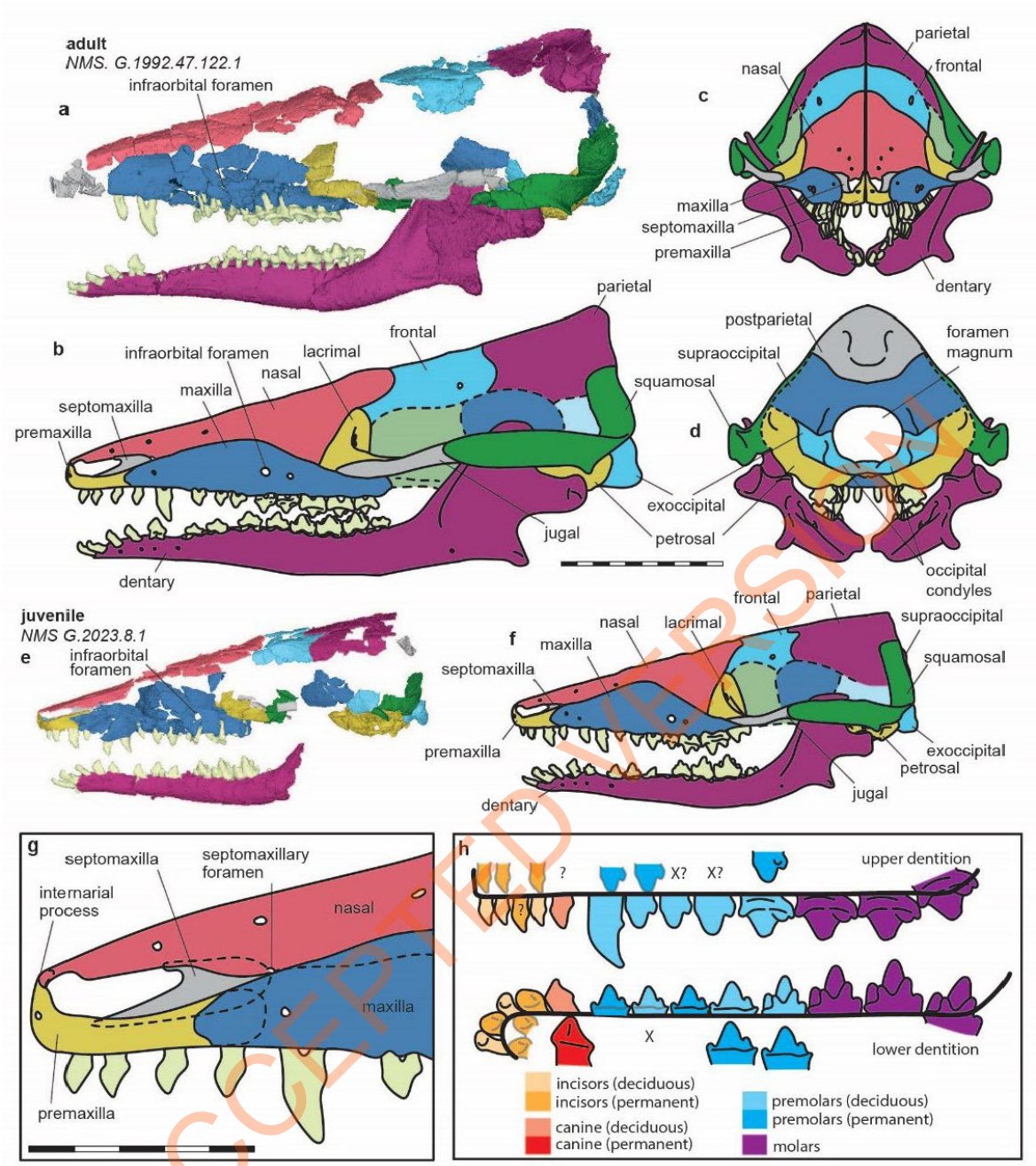

Extended Data Figure 2: Reconstructed skull of *Krusatodon kirtlingtonensis*. **a-d**, NMS. G.1992.47.122.1; **e-f**, NMS G.2023.8.1. **a** and **e**, left lateral view of digitally rendered skull elements, placed in anatomically correct positions. **b-d** and **f,** diagrammatic reconstructions of skull in: **b** and **f**, left lateral; **c**, anterior/rostral; **d**, posterior/caudal views. **g**, anterior portion of skull showing extent of elements with dotted lines. **h**, simplified diagram of teeth showing replacement stage in NMS G.2023.8.1. Scale bar same for **a-f** = 10 mm. Scale bar for **g** = 5 mm.

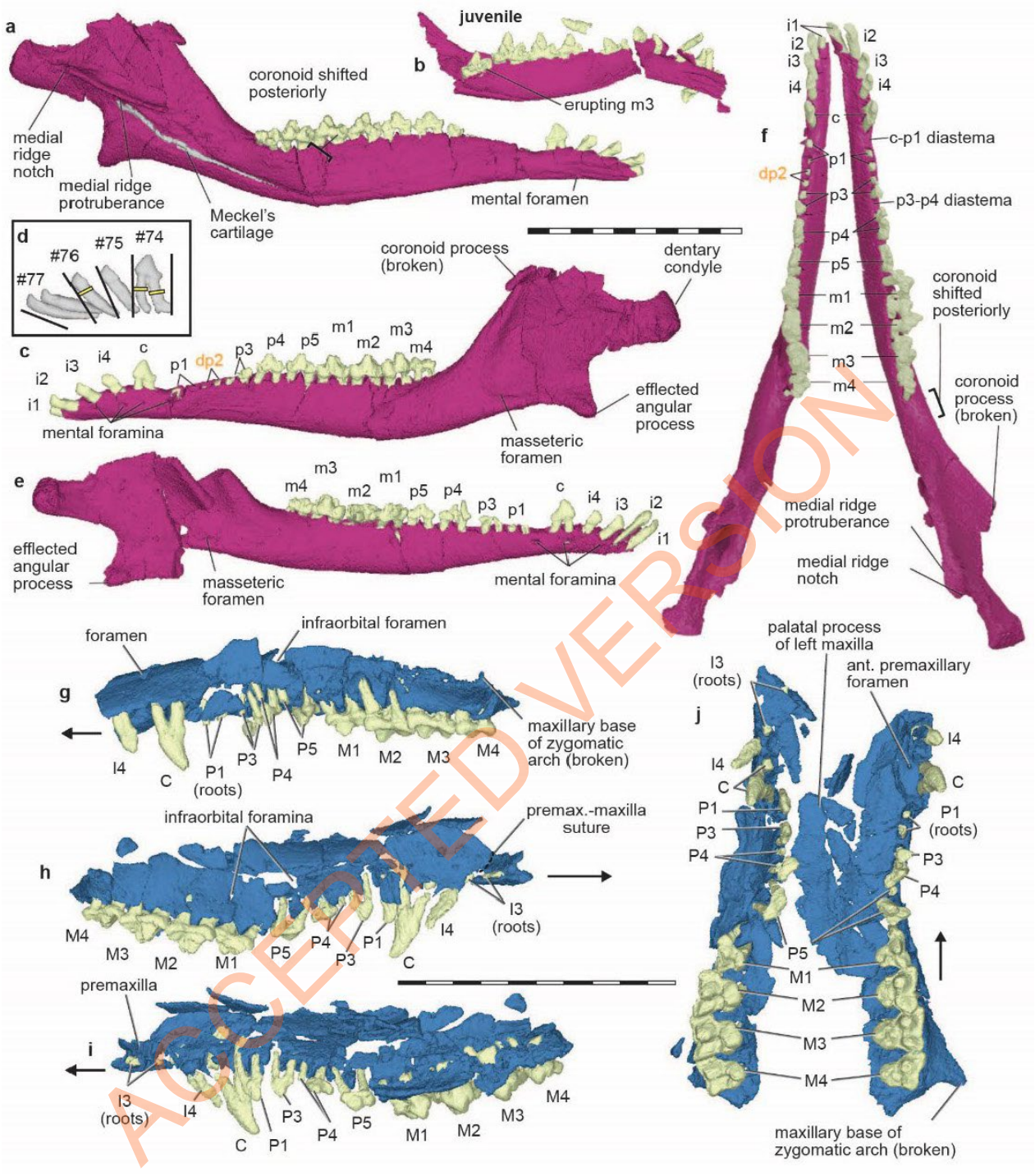

Extended Data Figure 3: Dentaries and maxillae of adult *Krusatodon kirtlingtonensis* NMS. G.1992.47.122.1. **a**, left dentary in medial view; **b**, left dentary of juvenile NMS G.2023.8.1 in medial view for comparison; **c**, left dentary in lateral view; **d**, location of dental cementum data for i1-c in specimen NMS G.1992.47.124, locations marked with yellow boxes, numbers correspond to Supplementary Table 8 and Supplementary Files; **e,** right dentary in lateral view; **f**, partially reconstructed dentaries in occlusal view; **g**, left maxilla in lateral view; **h**, right maxilla in lateral; **i**, and medial views; **j**, partial reconstruction of the maxillae in occlusal view. Scale same for **a-f**, and for **g-j**. All scale bars = 10 mm.

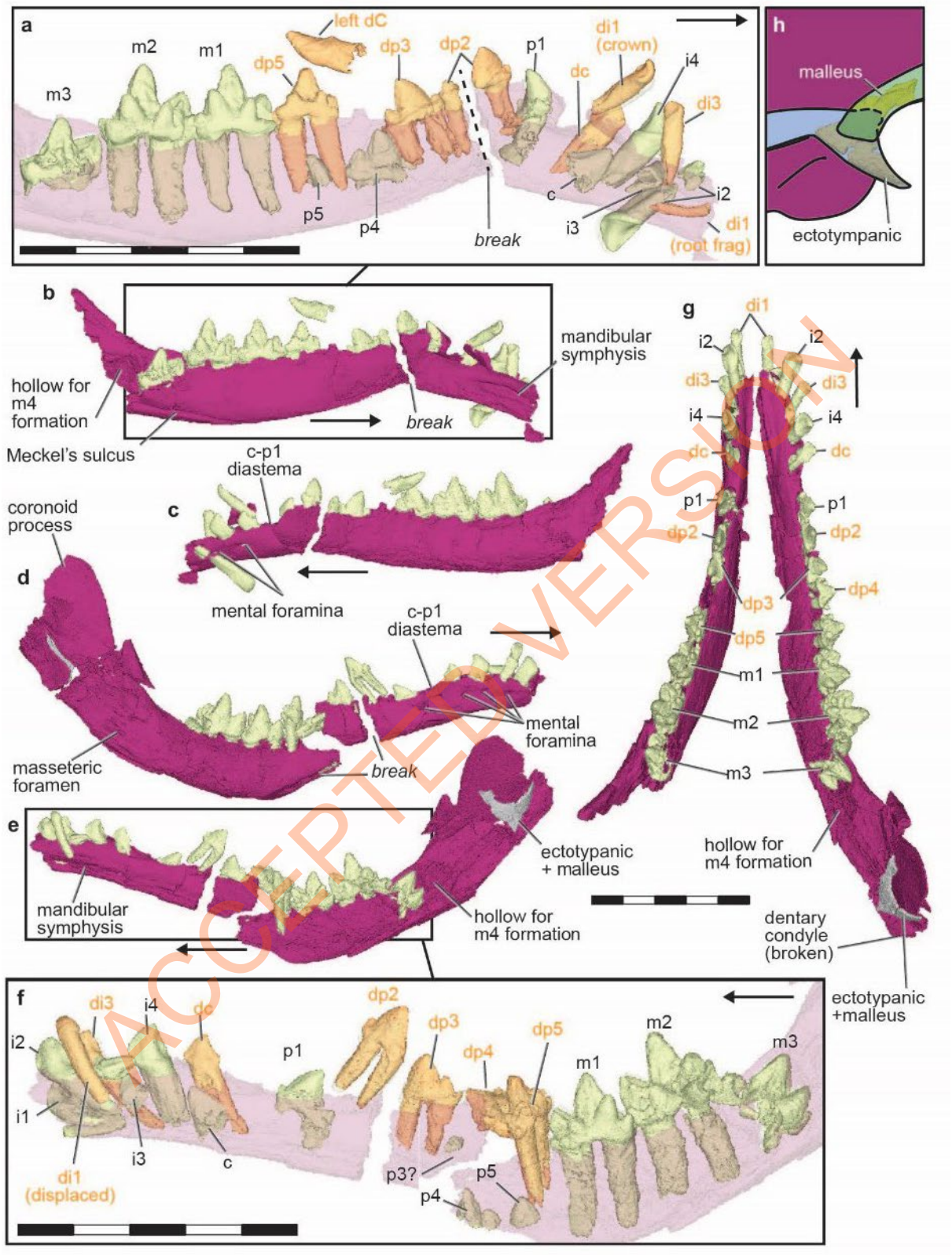

Extended Data Figure 4: Dentaries of juvenile *Krusatodon kirtlingtonensis* NMS G.2023.8.1. **a-c**, left dentary and teeth: **a**, lower tooth row in medial view showing deciduous (orange) and permanent generations; **b**, medial; **c**, and lateral views. **d-f**, right dentary and teeth: **d**, lateral; **e**, and medial views; **f**, lower tooth row in medial view showing deciduous (orange) and permanent generations. **g**, partially

reconstructed dentaries in occlusal view. **h**, diagrammatic reconstruction of postdentary bones. Arrows indicate anterior direction. Scale bar same for **b-e** and **g** = 10 mm. Scale bar for **a** and **f** = 5 mm.

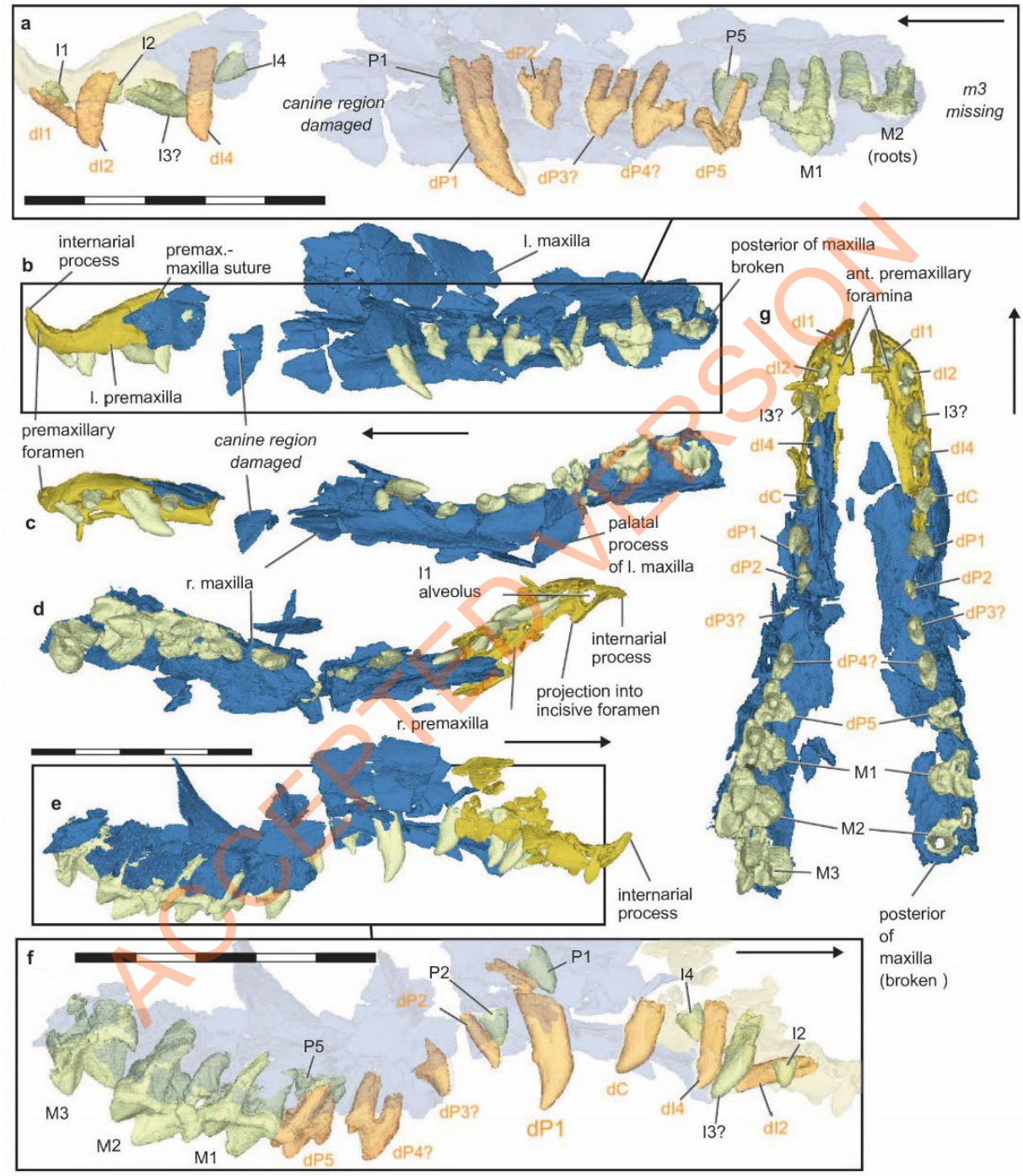

Extended Data Figure 5: Maxillae and premaxillae of juvenile *Krusatodon kirtlingtonensis* NMS G.2023.8.1. **a-c**, left maxilla and premaxilla: **a**, upper tooth row in lateral view showing deciduous (orange) and permanent generations; **b**, lateral; **c**, and occlusal views. **d-f**, right maxilla and premaxilla: **d**, occlusal; **e**, and lateral views; **f**, upper tooth row in lateral view showing deciduous (orange) and permanent generations. **g**, partial reconstruction of maxillae and premaxillae in occlusal view.

Arrows indicate anterior direction. Scale bar same in **b-e** and **g** = 10 mm. Scale bars in **a** and **f** = 5 mm.

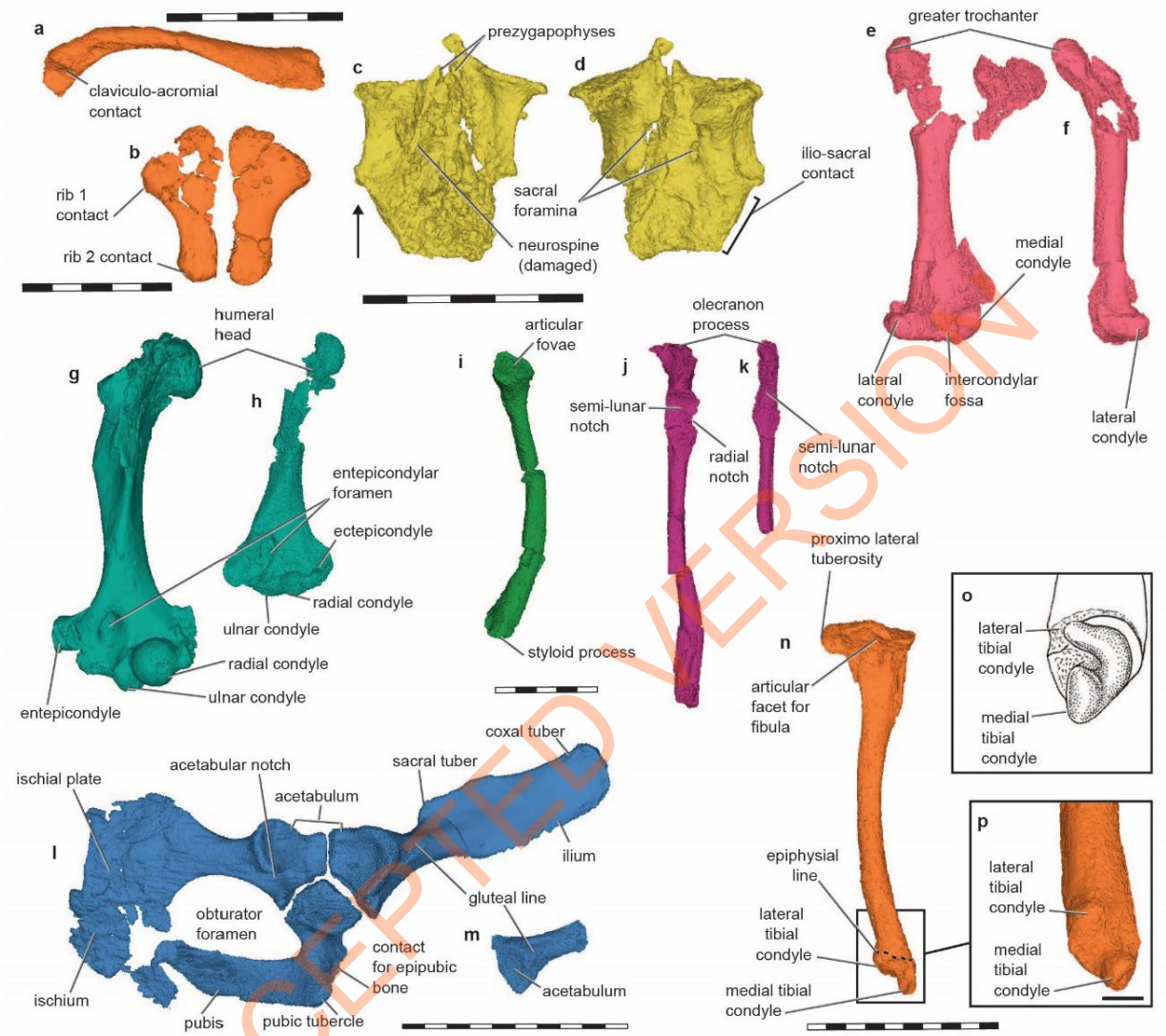

Extended Data Figure 6: Postcranial skeleton of *Krusatodon kirtlingtonensis*. **a-b**, **e-f**, **g**, **i-j**, **l**, **n** and **p**, adult NMS. G.1992.47.122.1. **c-d**, **h**, **k** and **m**, juvenile NMS G.2023.8.1. **a**, right clavicle; **b**, manubria; **c**, sacrum in dorsal view; **d**, sacrum in ventral view; **e**, left femur in posterior view; **f**, left femur in lateral view. **g-h**, left humeri in anterior view; **i**, left radius; **j-k**, left ulnae in anterior view; **l**, right pelvic girdle in lateral view; **m**, posterior of the right ilium in lateral view; **n**, left tibia in medial view; **o**, distal tibia in *Eucosmodon* adapted from Yuan et al. (2013); **p**, distal tibia showing condyles. Scale same for **i-k**. Scale bars **a-d** and **l-k** = 5 mm. All other scale bars = 10 mm.

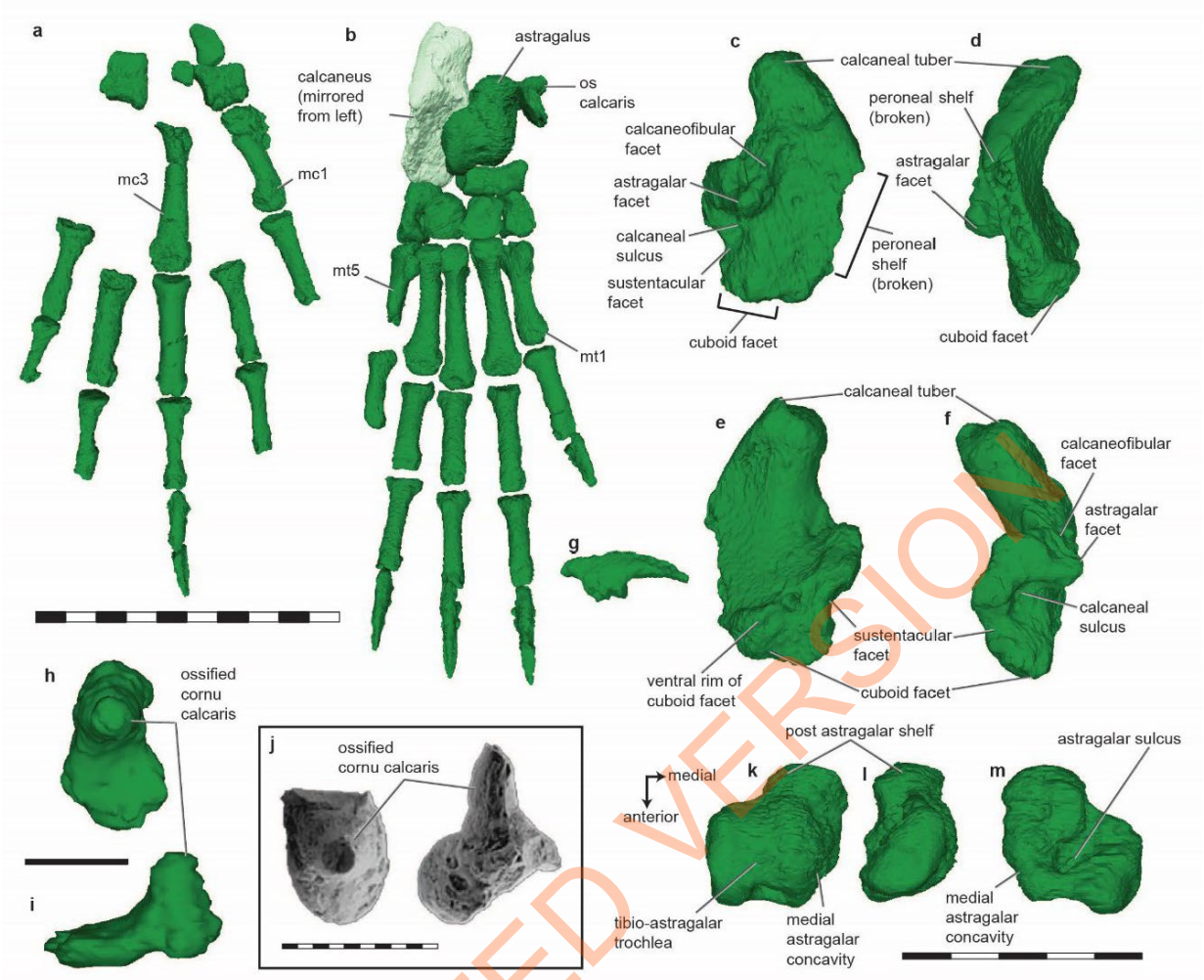

Extended Data Figure 7: Manus and pes of *Krusatodon kirtlingtonensis* NMS. G.1992.47.122.1. **a**, speculative reconstruction using preserved elements of right manus; **b**, speculative reconstruction using preserved elements of right pes, mirrored calcaneus in paler green. Only named elements have confident identifications, so all placements for other elements are speculative. **c-f**, left calcaneus in: **c**, dorsal; **d**, lateral; **e**, ventral; **f**, and medial views. **g**, example of ungual (position unknown); **h-i**, os calcaris; **j**, os calcaris in *Gobiconodon*, adapted from Hurum et al (2006). **k-m**, right astragalus in: **k**, dorsal; **l**, lateral; **m**, and ventral views. Scale same for **a-b** = 10 mm. Scale same for **c-g** and **k-l** = 5 mm. Scale in **h-i** = 5 mm. Scale in **j** = 10 mm.

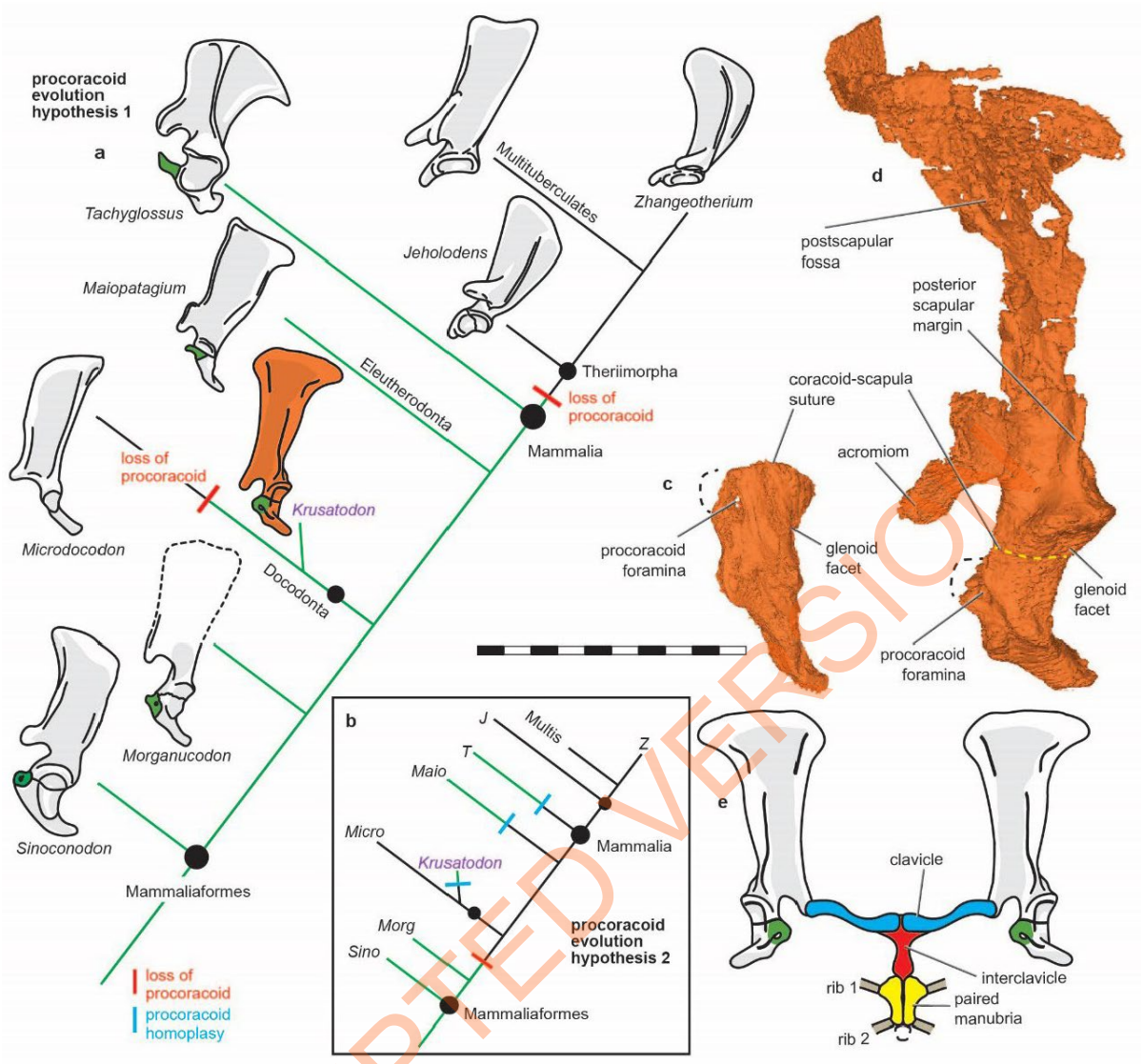

Extended Data Figure 8: Evolution of the mammaliaform procoracoid. **a**, the addition of information from *Krusatodon* suggests two independent losses of the procoracoid: once in Docodonta, and later in stem therians; **b**, an alternative hypothesis for shoulder evolution requires three homoplasies; **c**, incomplete scapulacoracoid of juvenile *Krusatodon* NMS G.2023.8.1; **d**, scapulacoracoid in adult *Krusatodon* NMS. G.1992.47.122.1; **e**, diagrammatic reconstruction of the pectoral girdle.

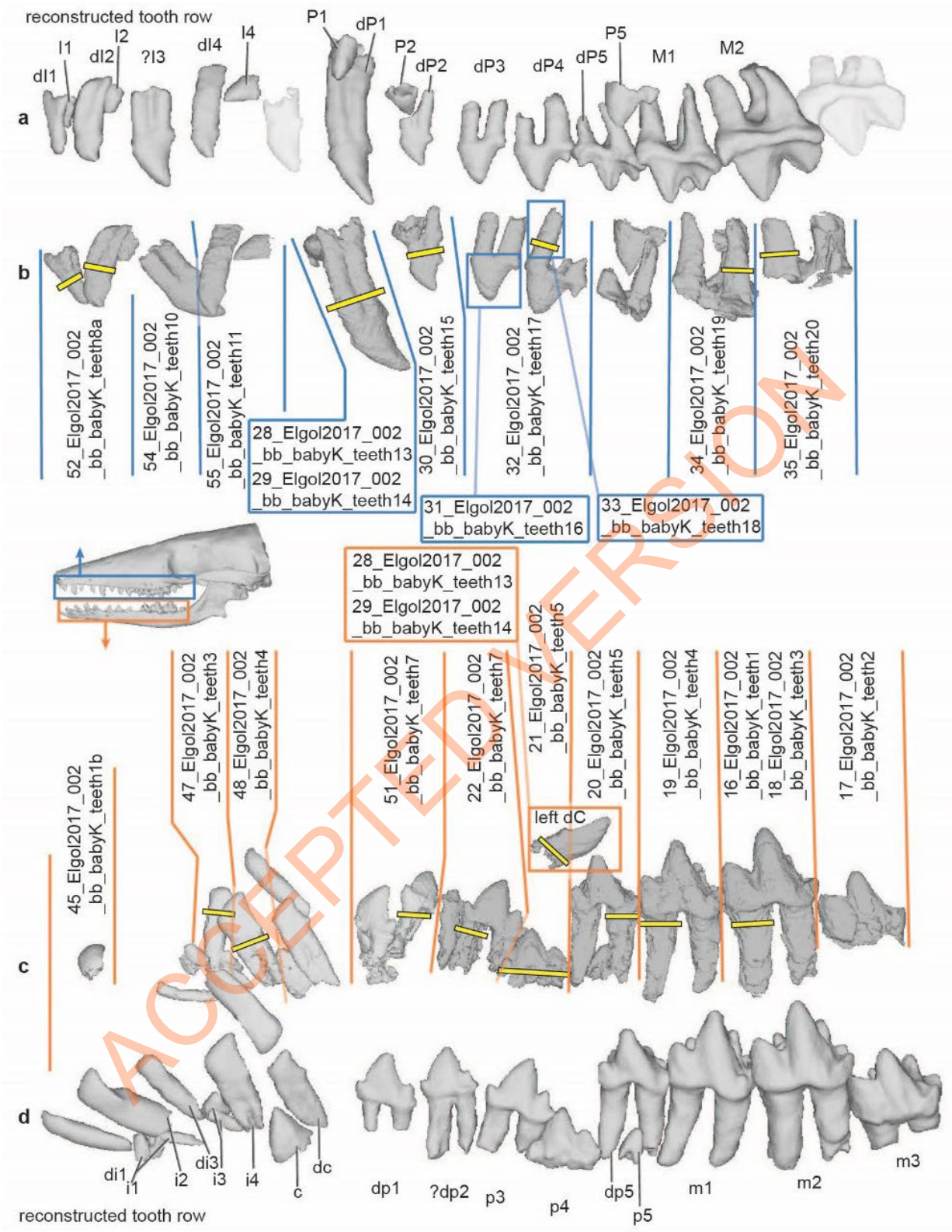

Extended Data Figure 9: Location of histological sections in the left tooth rows of juvenile *Krusatodon* NMS G.2023.8.1, indicated by yellow rectangles. **a**, left upper tooth row with loci labelled; **b**, left upper tooth row with locations of histological sections; **c**, left lower tooth row with locations of histological sections; **d**, left lower tooth row with loci labelled. Names of sections correspond to Supplementary Files.

See Figure 3-4 in main paper, and Supplementary Table 8 for cementum increment pair counts.

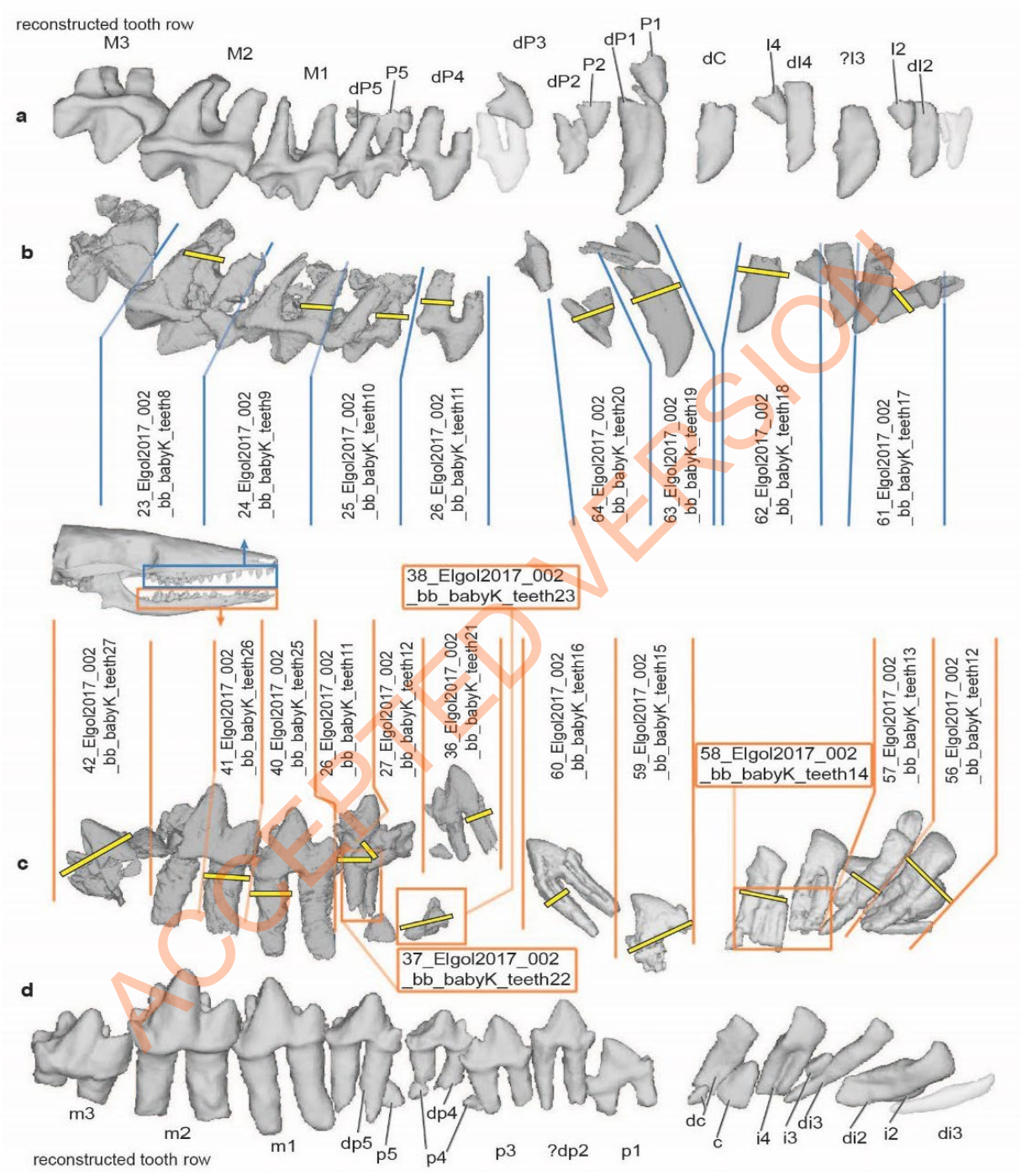

Extended Data Figure 10: Location of histological sections in the right tooth rows of juvenile *Krusatodon* NMS G.2023.8.1, indicated by yellow rectangles. **a**, right upper tooth row with loci labelled; **b**, right upper tooth row with locations of histological sections; **c**, right lower tooth row with locations of histological sections; **d**, right lower tooth row with loci labelled. Sections obtained using synchrotron tomographic

imaging. Names of sections correspond to Supplementary Files. See Figure 3-4 in main paper, and Supplementary Table 8 for cementum increment pair counts.